The mechanisms and functions underlying asymmetry in *Drosophila* neuroblasts

Melissa Delgado

A dissertation

submitted in partial fulfillment of the

requirements for the degree of

Doctor of Philosophy

University of Washington

2023

Reading Committee:

Clemens Cabernard, Chair

Charles Asbury

Julie Theriot

Linda Wordeman

Program Authorized to Offer Degree:

Biology

University of Washington

Abstract

The mechanisms and functions underlying asymmetry in *Drosophila* neuroblasts

Melissa Delgado

Chair of the Supervisory Committee:
Clemens Cabernard
Department of Biology

Asymmetric cell division (ACD) is a highly conserved developmental process utilized to create novel cell populations. ACD can be molecular, physical or a combination of the two. In molecular asymmetry, sibling cells inherit distinct sets of RNA or proteins while in physical asymmetry the sibling cells differ in their size. Although much is known about molecular asymmetry in regard to mechanisms and functions, physical asymmetry remains poorly understood. Thus, I sought to gain a better understanding of the establishment and role of physical asymmetry in *Drosophila* neuroblasts. Utilizing biochemical and fly genetic approaches to molecularly characterize the mechanism by which Protein Kinase N (Pkn) induces an apical to basal Myosin flow, over 50 potential binding partners of Pkn were identified. Initial characterization of a few selected top candidates including Lethal Giant Larvae, Shaggy, and

Twins showed a similar phenotype to *pkn* mutants. Thus, these candidates warrant additional analysis in order to determine whether they directly interact with Pkn.

To assess the functional consequences of altered physical asymmetry as well as molecular asymmetry, a nanobody approach was employed. Altering physical ACD by trapping Myosin to the apical cortex of neuroblasts resulted in symmetric as well as inverted asymmetric sibling cells. The changes to sibling cell size were found to alter cell fate via changes in cell cycle timing as well as the number and nuclear size of cells postulated to have a neuroblast fate. Thus, cell size alone can alter cell fate. Based on these results, I wondered whether inverting molecular asymmetry could also result in altered cell fate. Thus, I chose to trap the scaffolding protein Miranda, which shuttles the basal determinants Prospero and Brat to the basal cortex, to the apical cortex of neuroblasts utilizing a nanobody approach. In addition to Miranda's mislocalization, a portion of Prospero was found to be trapped to the apical cortex. Alterations to molecular asymmetry resulted in changes in cell cycle timing as well as the number and nuclear size of cells postulated to have a neuroblast fate. Although Miranda and a subset of Prospero was trapped apically, I found polarity to be maintained. Taken together, this research has demonstrated alterations in physical as well as molecular asymmetry can affect cell fate within *Drosophil*a neuroblasts. Thus, I have begun to elucidate the mechanisms and functions behind physical asymmetry.

TABLE OF CONTENTS

ACKNOWLEDGEMENTS

I would like to thank Dr. Cabernard for allowing the opportunity to work in his lab. Due to his guidance, I was able to develop an entirely new set of skills. My research would not be where it is today without my wonderful committee members. I would like to thank Dr. Asbury, Dr. Theriot and Dr. Wordeman for their insightful questions, scientific feedback, and interest in my personal as well as my professional development over the years. For their support, I am truly grateful. Additionally, I would like to thank my collaborators Dr. Davis and Dr. Zelter. Without their biochemical expertise, assistance with mass spectrometry and data analysis part of my thesis would never have come to fruition.

Throughout my PhD studies, I have been fortunate enough to have a loving husband to support me during the highs and lows. Thank you Mark for always being there for me! I would like to thank my parents for their unconditional love and instilling in me a strong work ethic. Completing a PhD takes a team and so I must thank a few more individuals. Thank you Juanje Vicente, Nicole Horsley, Adam Von Barnau Sythoff, Carlos Segura, Bharath Sunchu, and Jenny Taylor for brainstorming ideas, letting me blow off steam and in a lot of cases both.

Mechanical regulation of cell size, fate and behavior during asymmetric cell division

Melissa Delgado[1] & Clemens Cabernard[1]

[1]Department of Biology, University of Washington, Life Science Building, Seattle, WA 98195, USA

Published in Current Opinion in Cell Biology 2020, 67:9–16.

Abstract

Asymmetric cell division (ACD) is an evolutionary conserved mechanism used by prokaryotes and eukaryotes alike to generate cell diversity. ACD can be manifested in biased segregation of macromolecules or differential partitioning of cell organelles. Cells are also constantly subject to extrinsic or intrinsic mechanical forces, influencing cell behavior and fate. During ACD, cell intrinsic forces generated through the spatiotemporal regulation of the actomyosin cytoskeleton can influence sibling cell size. External mechanical stresses are further translated by transcriptional co-activators or mechanically gated ion channels. Here, we will discuss recent literature, exploring how mechanical cues influence various aspects of ACD and stem cell behavior, and how these mechanical cues contribute to cell fate decisions.

Introduction

Asymmetric cell division (ACD) is a conserved mechanism evolved to generate cellular diversity. A key principle of ACD is the establishment of distinct sibling cell fates by mechanisms linked to mitosis. Differential sibling cell fates can be acquired through biased segregation of macromolecules, differential partitioning of organelles, and/or variations in sibling cell size or shape [1]. ACD is preceded by symmetry breaking events, often induced through precise spatiotemporal regulation of the cytoskeleton. Modulating the contractility of actomyosin underneath the plasma membrane (cell cortex, hereafter) can induce cortex and membrane flows, affecting cytoplasmic streaming and/or influence hydrostatic pressure. These

intrinsic mechanical forces, generated by the cytoskeleton, can modify cell size, morphology, spindle orientation and positioning, all of which can ultimately impact cell fate bias. However, how mechanical and biochemical cues intertwine to induce symmetry breaking events is an open question in the field. Similarly, whether and how forces generated by the cytoskeleton directly translate into cell fate bias is unclear. Cells are also exposed to extrinsic mechanical cues such as substrate stiffness, shear stress, compression or intercellular adhesive forces, impacting cell morphology and size. How extrinsic cues are translated into cell fate bias during ACD remains to be resolved. Here, we will review recent literature on how cell intrinsic and extrinsic mechanical forces affect stem cells and ACD, focusing primarily on metazoans systems.

The mechanobiology of sibling cell size asymmetry

A clear manifestation of ACD is the formation of unequal sized sibling cells, here also referred to as physical or sibling cell size asymmetry. Sibling cell size asymmetry can be generated through various cell intrinsic mechanical forces such as: (1) asymmetric spindle positioning through cortical pulling or cytoplasmic pushing forces, (2) biased cortical expansion or (3) biased retraction of cortical lobes. Several recent studies illustrate how molecular modifications of the cytoskeleton result in symmetry breaking events, necessary to generate forces implicated in establishing sibling cell size asymmetry. For instance, in sea urchins, ACD is achieved through spindle displacement towards the vegetal cell cortex, generating micromeres and macromeres. Micromeres are smaller than their macromere sibling cells and inherit the RNA helicase protein Vasa. During the 8-cell stage, the proteins Activation of G-protein Signaling (AGS) and Galphai are present on the vegetal cortex and form a complex with NuMA, Dynein and Vasa. This complex displaces the spindle towards the vegetal cell cortex, while also accumulating Vasa. The animal spindle pole clusters phosphorylated PLK1, which appears to

disassociate NuMA, Dynein and Vasa. This reinforces the asymmetric spindle localization due to Dynein pulling on microtubules while simultaneously accumulating Vasa on the vegetal pole. AGS is both necessary and sufficient to establish this physical and molecular ACD (Figure 1a) [2]. This finding is consistent with a number of studies, showing that the core cortical force-generating machinery responsible for cortical pulling forces is evolutionary conserved and contains the Dynein-Dynactin complex, NuMA (Lin5 in *C. elegans*; Mud in *Drosophila*) and the Galphai complex (GOA-1, GPA-16 in *C. elegans*; Galphai in *Drosophila*) [3]. Artificial pulling of the mitotic spindle, using injected magnetic beads and a local magnetic field, towards one side of the cell cortex is sufficient to induce unequal sized sibling cells in sea urchin zygotes [4].

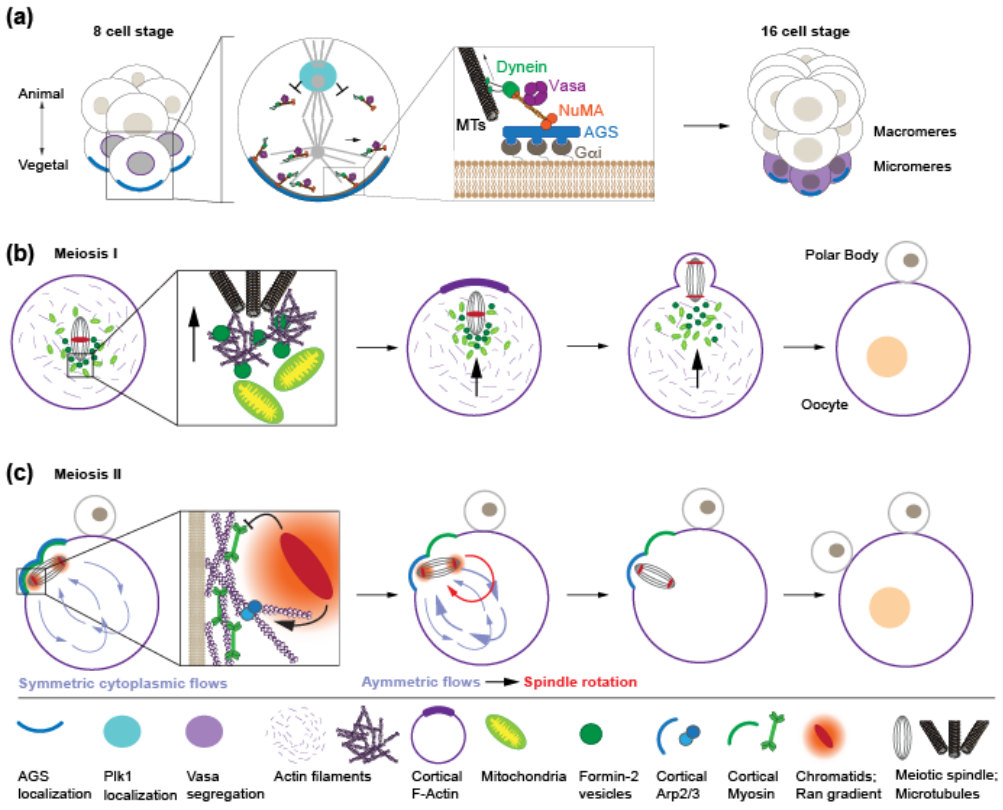

Figure 1

Figure 1: Spindle-dependent mechanisms inducing sibling cell size asymmetry
(a) After the establishment of the 8-cell embryo, AGS and Galphai are localized to the vegetal pole within the vegetal blastomeres. Vasa is localized in the nucleus. During metaphase, the spindle is pulled towards the vegetal cortex. This is achieved through cortical AGS and Galphai,

Figure 1 Continued: Spindle-dependent mechanisms inducing sibling cell size asymmetry **(a)** interacting with Dynein via NuMA. Vasa forms a complex with Dynein, NuMA, Galphai and AGS on the vegetal cortex but is excluded from the animal spindle pole through Plk1, which dissociates NuMA, Dynein and Vasa. This disparity between the two spindle poles reinforces asymmetric spindle localization, resulting in the formation of large macromeres and small, Vasa-containing micromeres. **(b)** During meiosis I in mouse oocytes, Formin-2 is present around the spindle allowing for the nucleation of F-actin on vesicles surrounding the spindle. This nucleation is essential for initial spindle movement. Additionally, these vesicles are surrounded by mitochondria which may be utilized as a method of force to push the spindle towards the cell cortex further escalating asymmetry. **(c)** After chromosome segregation during meiosis II in mouse oocytes, each pole has a separate actomyosin domain of influence resulting in symmetric hydrodynamic forces. However, these forces become unbalanced, due to the presence of RanGTP on the chromosomes. The RanGTP signaling results in the activation of Arp2/3 while simultaneously inhibiting Myosin at the cell cortex. Together these asymmetric hydrodynamic forces drive spindle rotation.

In most cell types, pulling forces are mediated by astral microtubules, interacting with the Actin-rich cytoskeleton beneath the plasma membrane [5]. However, meiotic spindles in mammalian oocytes lack canonical centriole-containing centrosomes and are devoid of astral microtubules that could form long-distance cortical connections. Mammalian oocytes undergo two consecutive ACDs, generating a large egg and two small polar bodies. The first physical ACD depends on Actin filaments nucleated by the Actin nucleators Formin-2 (FMN2) and the Arp2/3 complex, inducing a targeted migration of the meiotic spindle towards the actomyosin-rich cortex [6]. Mechanistically, this is achieved through spindle-periphery localized FMN2, nucleating short Actin bundles, most likely from endoplasmic reticulum-derived vesicles. These Actin filaments around the spindle periphery are surrounded by mitochondria and could induce directional spindle movement through a pushing force (Figure 1b) [7]. Subsequently, polar body formation is induced through Cdk1 inactivation, which triggers cytoplasmic FMN2-mediated F-actin polymerization that propels the spindle into the cortex, thereby inducing protrusion [8]. The second physical ACD is induced through cortical Actin-mediated spindle positioning and subsequent spindle rotation. The arrested meiotic metaphase spindle is overlaid by a cortical F-

Actin cap, formed by cortical Arp2/3, which generates a continuous Actin flow that drives cytoplasmic streaming, pushing the spindle towards that cap [9]. To complete the second meiotic division after fertilization, thus eliminating a set of sister chromatids through polar body formation, the spindle must rotate from a parallel to a radial orientation relative to the oocyte cortex. This spindle rotation in meiosis II is executed through an asymmetric cytoplasmic flow that is powered by asymmetrically localized Non-muscle Myosin II (hereafter Myosin) and Arp2/3 on the cortex above the spindle. Additionally, spindle rotation also depends on a central pivot point from the central spindlin-complex (Figure 1c) [10]. Displacement of the mitotic or meiotic spindle exposes the cell cortex to furrow inducing cues, completing the abscission of a small polar body or sibling cell [11].

A spindle-independent symmetry breaking event, used to generate physical asymmetry, induces biased cortical expansion and is utilized by *Drosophila* neuroblasts, the neural stem cells of the developing fly brain. *Drosophila* neuroblasts undergo repeated asymmetric cell divisions, generating a large self-renewed Neuroblast (Nb) and a small differentiating Ganglion Mother Cell (GMC); GMCs usually divide once more to create neurons and/or glia [12]. This sibling cell size asymmetry is established during anaphase onset, caused by an expansion of the apical cell cortex, shifting the cleavage furrow basally [13,14]. Apical cortical expansion is permitted by spatiotemporal Myosin) regulation, inducing first a basally directed, followed by an apically directed cortical Myosin flow. The symmetry breaking event, triggering the onset of Myosin flow towards the basal cortex is induced by the polarity protein Partner of Inscrutable (Pins; LGN/AGS3 in vertebrates), recruiting both Rho Kinase (Rok; Rok1-2 in vertebrates) and Protein Kinase N (Pkn; PKN1-3 in vertebrates). Subsequently, spindle-dependent cues induce a Myosin flow in the opposite direction, resulting in an accumulation of Myosin at the cleavage furrow.

This spatiotemporal regulation of Myosin activity has been shown to be sufficient to change physical asymmetry (Figure 2a) [13,15–17]. Recent stiffness measurements revealed that Nbs build-up hydrostatic pressure until early anaphase, before it drops again. This hydrostatic pressure initiates biased apical expansion due to a relief of apical Myosin contraction, impacting sibling cell size asymmetry establishment [18].

Unlike *Drosophila* Nbs, the onset of actomyosin flows in *C. elegans* zygotes utilizes the kinase Aurora-A around centrosomes to locally inhibit actomyosin contractility. This symmetry breaking event, dependent on Aurora-A's kinase activity, induces a Myosin flow towards the anterior cell cortex. Subsequently, Aurora-A also mediates global disassembly of cortical actomyosin, by suppressing the excitation of cortical Rho1, facilitating initial polarization through suppression of centrosome-independent cortical flows [19,20].

An interesting, but poorly investigated mechanism used to establish sibling cell size asymmetry occurs during spiralian development of mollusks and some annelid embryos. These invertebrates establish physical asymmetry via polar lobes, also known as antipolar or yolk lobes. Polar lobes are transient vegetal protrusions, forming during the first and second embryonic divisions, sequestering vegetal cytoplasm that is inherited by the CD and D blastomeres, respectively [21]. Toledo-Jacobo et al. found that in scallops, inhibition of Arp2/3 affects polar lobe formation and partitioning of cytoplasm into the two daughter cells, suggesting that Arp2/3 plays a functional role in defining the zone of cortex to be sequestered into the polar lobe [22]. The molecular mechanisms underlying polar lobe formation and retraction are currently unknown but classic microsurgery experiments revealed that polar lobes are instrumental in cell fate decisions (Figure 2b) [23–26].

How mechanical changes in physical cell size can affect cell fate is still unclear but has recently been examined in the worm [27]. *C. elegans* embryos establish anterior and posterior polarity gradients, via diffusion of PAR proteins. Theoretical modeling suggested the existence of a critical cell size threshold for polarity establishment. Smaller embryos – generated through genetic and physical manipulations - failed to stabilize polarity gradients inducing premature symmetric divisions [27].

These examples illustrate how cell intrinsic mechanisms and mechanical cues regulate sibling cell size asymmetry with potential implications on cell fate and behavior.

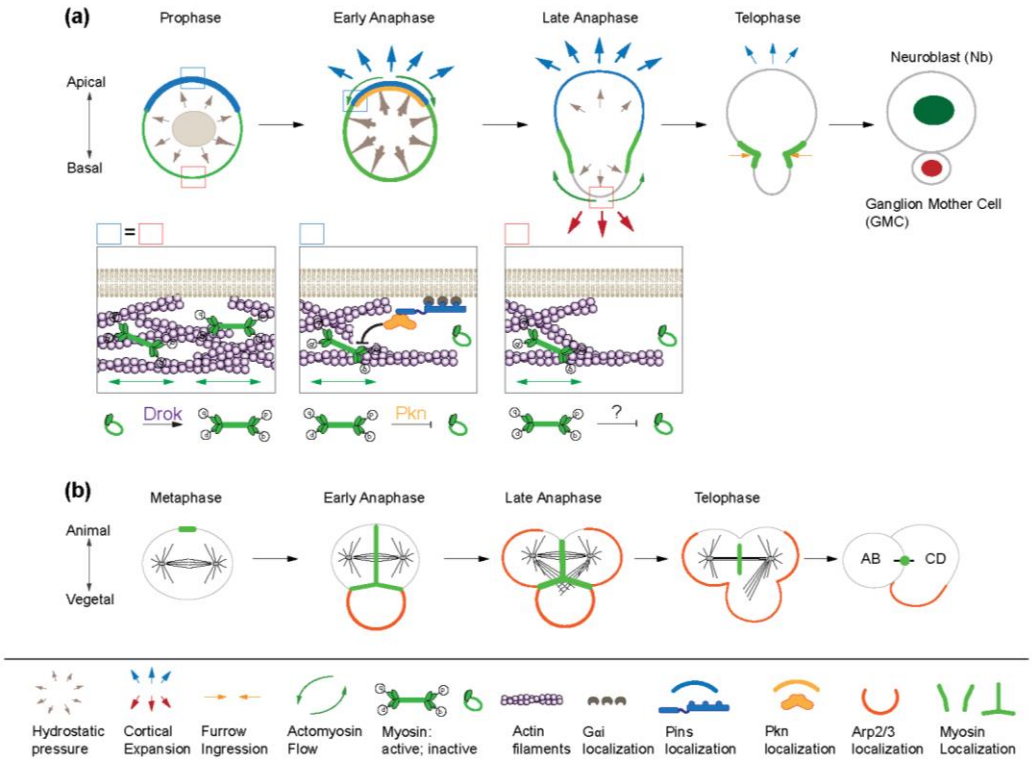

Figure 2

Figure 2: Spindle-independent symmetry breaking events, inducing sibling cell size asymmetry

(a) The interplay of biased Myosin relocalization and build-up of hydrostatic pressure initiates the establishment of physical asymmetry in fly neural stem cells (neuroblasts). Active cortical tension is isotropically distributed in prophase. In early anaphase, apical cortical tension is downregulated; Pins recruits Pkn apically, which is necessary for local Myosin inactivation. The resulting anisotropy in active tension results in a basally directed Myosin flow, relieving the

Figure 2 Continued: Spindle-independent symmetry breaking events, inducing sibling cell size asymmetry
(a) apical cell cortex of Myosin contraction. This built-up hydrostatic pressure dissipates apically, the cell cortex and membrane outwardly expand. Subsequently, spindle-dependent cues direct an apical Myosin flow towards the cleavage furrow. The mechanisms resulting in basal Myosin inactivation are unclear. Myosin contraction at the contractile ring allows for continued apical and basal cortical expansion.
(b) In scallops, Myosin enriches at the future cleavage furrow site as well as the future polar lobe construction site. Additionally, Arp2/3 becomes enriched on the polar lobe cortex. Arp2/3 subsequently also enriches on the animal cortex but retains its presence on the polar lobe cortex. Towards the end of cytokinesis, the polar lobe reintegrates into one sibling, giving rise to the larger CD cell.

Mechanosensation and cell fate responses *in vivo*

How asymmetrically dividing cells sense, transmit and interpret mechanical cues is unclear but mechanosensitive ion channels and transcriptional co-activators provide a conceptual framework. For instance, mechanical cues can be transmitted by the Actin cytoskeleton via the co-activators YAP and TAZ, translating mechanical stresses into transcriptional responses [28]. In the early mouse blastocyst, a symmetry-breaking event bifurcates the first cell lineages, creating the inner cell mass (ICM) and the outer extra-embryonic trophectoderm (TE). Subcellular localization of YAP is known to distinguish ICM and TE fates; nuclear YAP present in outer cells is essential for TE-fate maturation but remains cytoplasmic in inner cells [29]. YAP localization depends on Angiomotin (Amot), which binds both Actin and YAP [28]. Amot's localization can be controlled by substrate stiffness [30,31] but in pre-implantation mouse embryos, AMOT and YAP localization depends on cell polarity and not cell adhesion [32]. In mouse blastocysts, the apical domain has been shown to be sufficient for the first lineage segregation in which daughter cells inherit the apical domain adopt a trophectoderm fate. Amot colocalizes with the apical domain and induces nuclear YAP localization. While apical domains are subject to cortical tension [33,34], it has been proposed that cells with greater apical tension

tend to have higher levels of nuclear YAP/TAZ and a larger cell volume [35]. How YAP enters the nucleus is unclear in this system but could be induced through coupling of the nucleus and the Actin cytoskeleton, impacting nuclear pore size [36].

Another important determinant of mechanosensitive lineage selection is the mechanically gated ion channel Piezo1. Piezo1 can be activated by traction forces, inducing an inflow of Ca^{2+} in a substrate stiffness dependent manner. Additionally, Piezo1 has been proposed to be a homeostatic sensor, controlling epithelial cell numbers [37–39].

A recent report implicated Piezo in the mechanical regulation of intestinal stem cells (ISCs) in the fly midgut [40]. Adult *Drosophila* ISCs use a combination of extrinsic and intrinsic polarity cues to divide asymmetrically, generating an undifferentiated enteroblast (EB), which directly differentiates into a large epithelial-like, an absorptive enterocyte (EC) or a hormone-secreting enteroendocrine (EE) cell [41–43]. A subset of ISCs, destined to generate EEs, express the *Drosophila* orthologue Piezo, required for the generation of EE cells and sufficient to induce cell proliferation and EE cell differentiation. These findings suggest that at least a subset of *Drosophila* midgut stem cells directly sense mechanical signals through Piezo [40]. How mechanical forces activate Piezo is still under investigation and one possible mechanism involves the phosphorylation of Myosin by Myosin Light Chain Kinase [44].

Extracellular forces influencing oriented and asymmetric cell division

In multicellular contexts, a dividing cell receives numerous physical and chemical cues from multiple neighboring cells, influencing the final division axis and the position of the resulting sibling cells. For instance, during early development of *C. elegans* and mouse embryos, physical contact was shown to orient cell division and Myosin flow. Physical contact induces Myosin's anisotropic flows, sufficient to generate membrane movements, resulting in a cell surface torque

that orients the cell division axis [45]. Similarly, asymmetry in cell contacts in the mouse blastocyst directs the formation of an apical domain on the contact-free surface of outside cells, which is necessary and sufficient for TE differentiation [46]. Subsequent cell positioning can be achieved through cell sorting or oriented cell division. Cells destined to become ICM can be generated by inward cell sorting based on differential cortical tension [33,34] or through ACD [47,48]. Recent data suggests that oriented cell division does not influence cell fate but determines the segregation of the apical domain, which contributes to cell sorting [46]. Oriented cell division is determined by proper spindle orientation, which can be controlled through cell polarity, cell geometry, tricellular junctions and cortical tension [3,49]. *In toto* live cell imaging of the early mouse embryo revealed that cells stretched along the embryo surface undergo symmetric division, inducing other surface cells to change shape accordingly and divide asymmetrically. Conversely, cells with a longer apico-basal axis undergo asymmetric division guided by the apical domain, thereby stretching neighboring cells and prompting them to divide symmetrically. The interplay between cell shape and polarity ensures appropriate partitioning of ICM and TE cells, resulting in robust patterning of the blastocyst [50].

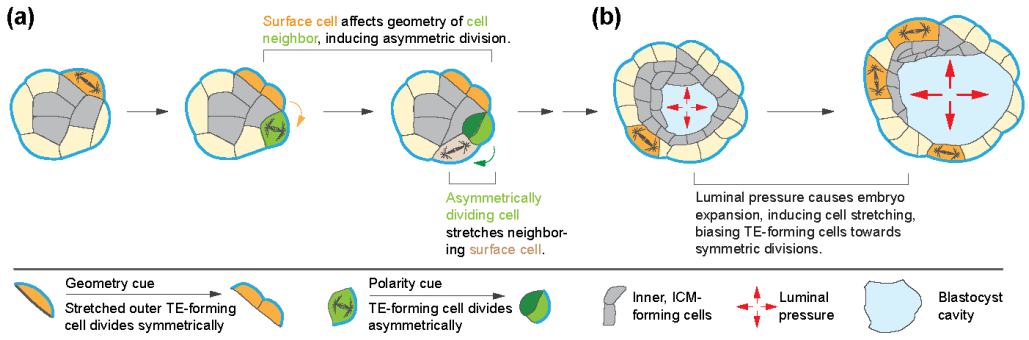

Figure 3

Figure 3: The contribution of mechanical forces to asymmetric cell division in the mammalian embryo

(a) Cell geometry and cell polarity both influence oriented cell division in the early mouse embryo. Surface tension stretches cells on the embryo surface, overriding intrinsic polarity cues

Figure 3 Continued: The contribution of mechanical forces to asymmetric cell division in the mammalian embryo
(a) (blue cortex). Stretched cells predominantly divide symmetrically, giving rise to two trophoectodermal cells. These symmetric divisions can alter the geometry of neighboring cells, so that polarity cues become the main determinant of spindle orientation. Cells oriented along the apico-basal cell axis result in asymmetric divisions, which place one sibling cell towards the inside of the blastocyst. Asymmetrically dividing cells can also stretch surface cells, inducing symmetric divisions. **(b)** Later during mouse development, a fluid-filled cavity is creating luminal pressure, which alters the cell geometry of blastocyst cells, triggering symmetric cell divisions.

Drosophila Nbs largely rely on cell-intrinsic polarity cues to orient the mitotic spindle but a recent report found that the last-born daughter cell is necessary to maintain a constant division axis over multiple subsequent cell divisions. The underlying mechanisms are unclear but could allow Nbs to maximize their contact area with glial cells known to provide protective and proliferative signals [51].

As the mouse embryo develops and increases in size, global changes in tissue mechanics and morphology further modify cell behavior and fate through mechanotransduction. For instance, a fluid-filled cavity forms and expands in the mouse blastocysts. This expansion causes the cells in the embryo to segregate into the extra-embryonic TE, lining the fluid-filled cavity, and the inner cell mass. An increase in hydrostatic pressure leads to lumen expansion and stretching of TE cells. These changes trigger increased cell contractility, resulting in tight junction maturation and expansion of the blastocyst to accommodate lumen growth. Changes in luminal pressure and size can influence the cell division pattern of the TE, affecting cell allocation and fate [52].

Conclusions

The influence of mechanical forces on cell fate has now been explored in various cell types and cell contexts. However, how these forces are sensed and ultimately relayed demands further exploration. Additionally, how mechanical forces specifically influence or regulate symmetry

breaking events under physiological conditions needs to be defined. To this end, tools must be established to measure, manipulate and/or induce mechanical forces *in vivo*. Furthermore, to clearly delineate whether mechanical forces directly influence cell fate decisions during ACD, cellular and subcellular processes must be dissected with high spatiotemporal control and monitored with sophisticated imaging methods. New optogenetic tools in combination with improved imaging and analysis methods will expand the boundaries of this exciting and emerging field.

Cell size contributes to cell fate in asymmetrically dividing *Drosophila* neuroblasts

Melissa K Delgado[1], Alex Zelter[2], Trisha N Davis[2], Clemens Cabernard[1]

[1]Department of Biology, University of Washington, Seattle, WA 98105, USA

[2]Department of Biochemistry, University of Washington, Seattle, WA 98105, USA

Abstract

Asymmetric cell division (ACD) is a highly conserved process used to create unique cell populations. ACD can be molecular, physical or a combination of the two. In molecular asymmetry, sibling cells inherit distinct sets of macromolecules or organelles while in physical asymmetry sibling cells differ in their size. Although ACD has been widely studied, the molecular mechanisms as well as the functions behind physical asymmetry remain poorly understood. Using both biochemical and fly genetics approaches to molecularly characterize the mechanism by which Protein Kinase N (Pkn) induces an apical to basal Myosin flow in *Drosophila* neuroblasts. We identified over 50 potential binding partners to Pkn and 3 of these candidates Lethal Giant Larvae, Shaggy, and Twins, warrant further investigation. Based on initial characterization of *shaggy* and *twins* RNA interference lines as well as previously published data from *lethal giant larvae* mutants, all exhibited a similar phenotype to *pkn* mutants. Additionally, the functional consequences of altered physical asymmetry or molecular asymmetry were examined utilizing a nanobody approach. By trapping Myosin to the apical cortex of neuroblasts physical ACD was altered resulting in symmetric as well as neuroblasts exhibiting inverted asymmetry relative to controls. Changes in sibling cell size were found to alter cell fate via changes in cell cycle timing as well as number of cells and nuclear size of cells postulated to be neuroblasts based on molecular marker expression. Likewise, molecular asymmetry was altered by trapping the scaffolding protein Miranda to the apical cortex of

neuroblasts. In addition to Miranda trapping, a small portion of Prospero was also found to relocalize to the apical cortex. In these cells with altered molecular ACD, we observed changes in cell cycle timing as well as the number of cells and nuclear size of cells postulated to have a neuroblast fate while continuing to maintain polarity. Overall, we propose Lethal Giant Larvae, Shaggy, and Twins bind to Pkn to provide the polarity-induced cues required for symmetry breaking. Taken together, altering sibling cell size can affect cell fate in *Drosophila* neuroblasts.

Introduction

Asymmetric cell division (ACD) is an important developmental process used to create cellular diversity in a numerous organisms including bacteria, insects, mammals and plants [53–57]. ACD can take many forms to give rise to two sibling cells with different cell fates. One form is recognized by the difference in sibling cell size, also known as sibling cell size asymmetry or physical asymmetry [55,58]. Another form is recognized by the unequal segregation of molecular determinants, such as mRNAs, organelles, and proteins, into the sibling cells [55,58]. Changes to molecular and/or physical ACD can affect the fate of the sibling cells as well as the fates of their progenitors, which may result in developmental defects, cancer or other diseases [59–61]. For instance, if the first embryonic division plane in *C. elegans* is altered, this compromises the cell fate of endodermal and pharyngeal lineages [62]. Additionally, in human glioblastoma cells, asymmetric accumulation of EGFR and p75NTR provide continued stemness cues resulting in further tumorigenesis [63]. Although much is known about the mechanisms and functions of molecular ACD, little is known regarding the establishment and physiological role of sibling cell size asymmetry. In our study we sought to gain a better understanding of physical asymmetry by addressing two questions: 1) What are the molecular mechanisms behind physical asymmetry? 2) What is the function of physical and molecular asymmetry?

The mechanism used to achieve physical asymmetry in organisms varies but is known to require cell intrinsic mechanical forces [64]. In sea urchins, spindle displacement towards the vegetal cell cortex in blastomeres results in the formation of large macromeres and small micromeres. Thus, to establish small micromeres, the spindle is displaced in blastomeres during the 8-cell stage. Specifically, AGS (human LGN and AGS3) and Galphai are localized to the vegetal cortex and complex with NuMA, Dynein as well as Vasa (human eIF4A) [2]. The accumulation of vegetal Vasa allows for molecular asymmetry in the micromeres via asymmetric translation. In other organisms, cytoskeletal related proteins play a role. For instance, mouse oocytes, undergo two rounds of physical asymmetry to establish the oocyte and polar bodies. In Meiosis I, Formin-2 vesicles around the mitochondria allow for the relocation of the spindle towards the cell cortex due to F-actin nucleation [7]. In Meiosis II, Ran gradients at the poles of the separated chromatids allow for asymmetric Arp2/3 activation and repression of non-muscle Myosin resulting in cytoplasmic flows sufficient enough to realign the spindle [9,10]. The consequence of this realignment is physical asymmetry, establishing a large oocyte and small polar body.

Recent research has identified a role for Actin and Myosin in physical asymmetry. Polarized Actin's spatiotemporal dynamics have been found to be critical for the establishment of ACD in *Drosophila* sensory organ precursor cells [65]. In the case of the *C. elegans* zygote, AIR-1's (human Aurora Kinase A) presence on the centrosome inhibits local actomyosin contractility [19]. This along with global suppression of cortical actomyosin and spindle displacement result in a large AB cell and a small P1 cell. Furthermore, in *C. elegans* zygotes, a physical cell size threshold is required for proper cell fate including pharyngeal and germline [27,62,66]. Additionally, *C. elegans* Q neuroblasts actomyosin dynamics are also crucial for proper ACD

[67,68]. Although spindle placement and actomyosin dynamics seem to be critical for establishing ACD in numerous systems, the cues required for symmetry breakage and the consequences of altered physical asymmetry on a cell and organismal level require further investigation.

Drosophila neural stem cells, also known as neuroblasts, provide a great model to examine the mechanisms and functions of physical asymmetry. In neuroblasts, physical asymmetry is established via actomyosin contractility and hydrostatic pressure generating a large self-renewing neuroblast and a small differentiating Ganglion Mother Cell [14,16–18]. Specifically, Myosin dynamics are regulated by both polarity-dependent and spindle-dependent cues [13–17]. The polarity-dependent pathway contains apically localized Pins (human LGN), which is necessary for the recruitment of Rho Kinase as well as the poorly characterized serine-threonine kinase, Protein Kinase N (Pkn) (human Pkn 1-3) [17]. Together these kinases induce the apical-basal flow of Myosin in early anaphase. Subsequently, spindle-dependent cues activate the small GTPase Rho at the cleavage furrow, inducing a Myosin flow, from the basal cortex laterally towards the cleavage furrow [15,16]. During mitosis, hydrostatic pressure peaks during in early anaphase coinciding with apical Myosin clearing [18]. Thus, hydrostatic pressure can expand the membrane on the apical cortex first, solidifying the establishment of sibling cell size asymmetry.

Here, biochemistry and fly genetics were utilized to molecularly characterize the mechanism by which Pkn induces and apical to basal Myosin flow. We confirmed via a *pkn* mutant that Pkn is indeed required for proper Myosin spatiotemporal dynamics. Additionally, over 50 potential binding partners of Pkn via mass spectrometry were identified. Based on initial knockdown examination as well as searching previously published data, 4 proteins including A Kinase Anchoring Protein 200 (no human ortholog), Lethal Giant Larvae (human LLG1L), Shaggy

(human GSK3B) and Twins (human PPP2R2D) exhibit apical Myosin enrichment similar to *pkn* mutants. We further investigated the functional consequences of altered sibling cell size asymmetry using a nanobody approach. Alterations in physical ACD, by trapping Myosin to the apical cortex of neuroblasts, can result in symmetric and inverted asymmetric sibling cells. This change in cell size can alter cell fate via changes in cell cycle timing. Additionally, the number as well as nuclear size of cells postulated to have a neuroblasts fate were lower in Myosin trapped brains. Likewise, altering molecular ACD by trapping the scaffolding protein Miranda to the apical cortex of neuroblasts and as a result lead to the trapping of Prospero. Changes to molecular ACD resulted in alterations in cell cycle timing as well the number as well as nuclear size of cells postulated to have a neuroblasts fate. However, polarity is still maintained in these cells.

In conclusion, we have begun to identify and characterize potential Pkn binding partners which may underline the molecular mechanisms required to break symmetry thus ensuring proper establishment of sibling cell size asymmetry. We have discovered that alterations to physical asymmetry can alter cell fate in *Drosophila* neuroblasts. We propose the mechanisms behind sibling cell size asymmetry as well as the functions of asymmetry may be conserved in other organisms that undergo ACD.

Results

Pkn is Required for Proper Spatiotemporal Dynamics of Myosin

In *Drosophila* neuroblast ACD, Pkn is required for proper spatiotemporal dynamics of Myosin [17]. Loss of Pkn function, pkn^{06736}, has been found to cause aberrant changes in cell shape [17]. Utilizing a mutant fly line, *pkn1T,* postulated to contain a truncated kinase domain (TKD) which reduces overall Pkn levels, we sought to confirm this published phenotype [69]. Live cell

imaging on third instar larvae was conducted and Myosin dynamics, via Sqh::GFP (human MYL9), in neuroblasts containing the Pkn TKD in a null background as well as wildtype neuroblasts from prophase to telophase were observed. As previously reported, we found Myosin enrichment on the lateral and basal cortexes to be reduced prior to nuclear envelope breakdown in Pkn TKD neuroblasts (Figure 1A & B) [17]. Additionally, Myosin's apical enrichment was prolonged until anaphase onset (Figure 1A & B) [17]. The duration of Myosin apical enrichment was also found to be significantly longer than that observed in wildtype neuroblasts (Figure 1C).

Neuroblast shape changes have been described in *pkn* mutants and we found Pkn TKD neuroblasts exhibit changes as well. Due to basal expansion occurring first immediately followed by apical cortex enlargement, transient inverted asymmetry was observed until anaphase at which point Myosin shifted laterally resulting in normal ACD (Figure 1A & B). We conclude Pkn is required for proper spatiotemporal dynamics of Myosin during ACD and its kinase domain may play a role.

Identification of Pkn's Potential Binding Partners

To gain a better understanding of the molecular mechanisms underlying sibling cell size asymmetry, we sought to identify Pkn's prospective binding partners. Presently in *Drosophila*, Pkn is only known to directly interact, via protein-protein interaction, with Downstream of Receptor Kinase (Drk) (human GRB2), Rac1 (human RAC1) and Rho1 (human RHOA) [70–72]. Additionally, in *Drosophila* neuroblasts, Pins has been found necessary for Pkn's apical localization [17]. To examine this, we first sought to make an endogenously C-terminally eGFP tagged Pkn *Drosophila* line via CRISPR. As previously reported utilizing the Pkn N-terminally tagged eGFP protein trap line $pkn^{CC01654}$, in neuroblasts Pkn localizes to the apical cortex during early metaphase (180s) and enrichment occurs during late metaphase (360s) (Figure 2A). During

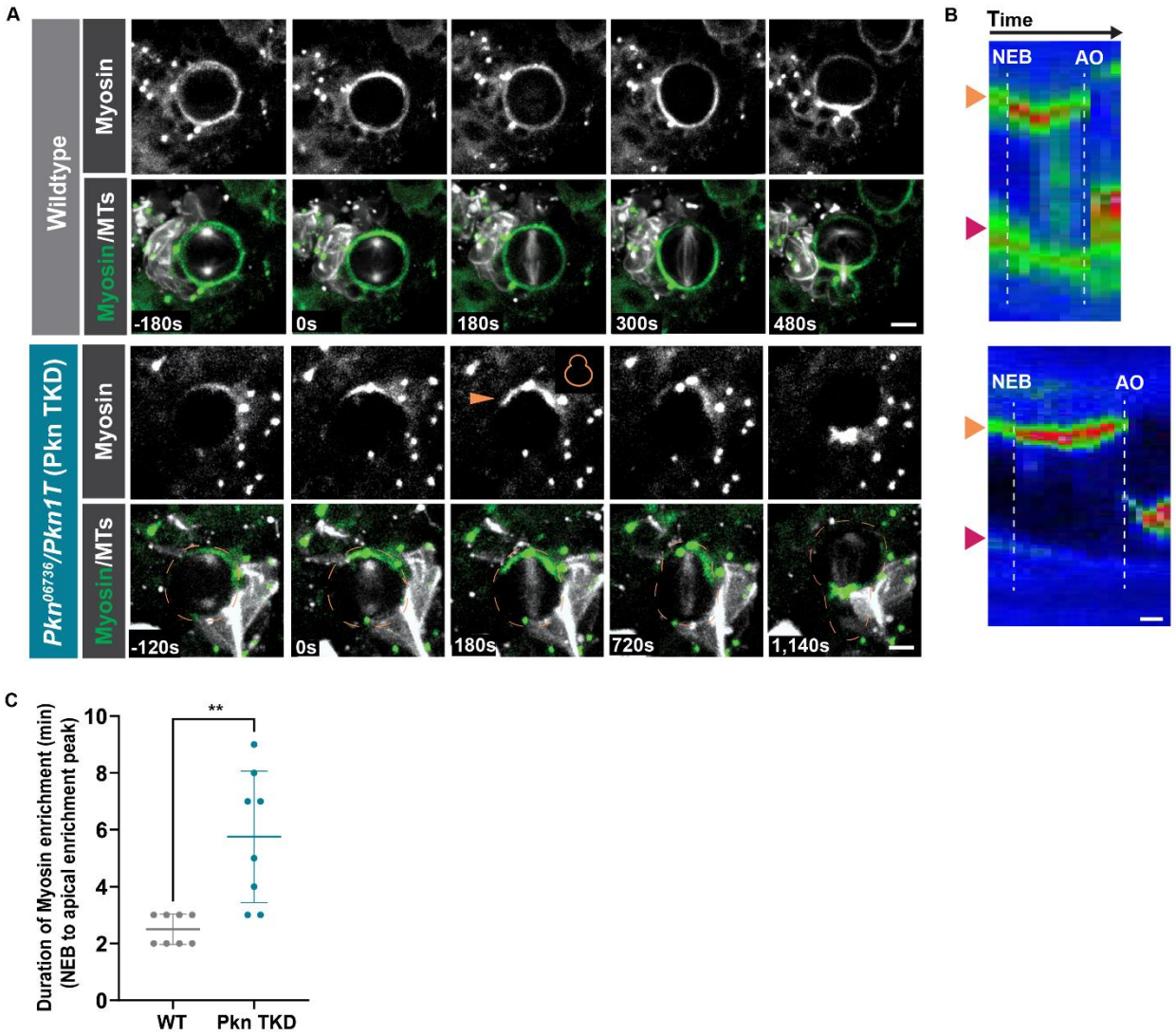

Figure 1: Pkn is Required for Proper Spatiotemporal Dynamics of Myosin
A. Representative image sequence of wildtype and *pkn*^{06736}(null allele)/*pkn1T* mutant third instar neuroblasts expressing Sqh::GFP (Myosin) and mCherry::Jupiter (microtubules; MTs). Wildtype (WT). *pkn1T*= Pkn Truncated Kinase Domain (TKD). Scale bar 4um. Time 0s is set to nuclear envelope breakdown. Orange dashes circle around Pkn TKD neuroblast through mitosis in dual channel panel. Orange arrow represents apical Myosin enrichment. **B.** Representative kymographs from neuroblasts shown in panel A. Kymographs made along the apical to basal cortex. Arrowheads highlight the apical (orange) and the basal (magenta) cortex, respectively. The vertical dashed lines refer to the nuclear envelope breakdown (NEB) and anaphase onset (AO). 4 pixels/min scale bar. Intensity ranges are indicated by Rainbow LUT. **C.** Bar graph of duration of Myosin enrichment in min for WT and Pkn TKD third instar neuroblasts.

anaphase (630s), Pkn becomes localized to the lateral cortex (Figure 2A). While at telophase

(810s), Pkn is localized to the cleavage furrow (Figure 2A). After division is complete,

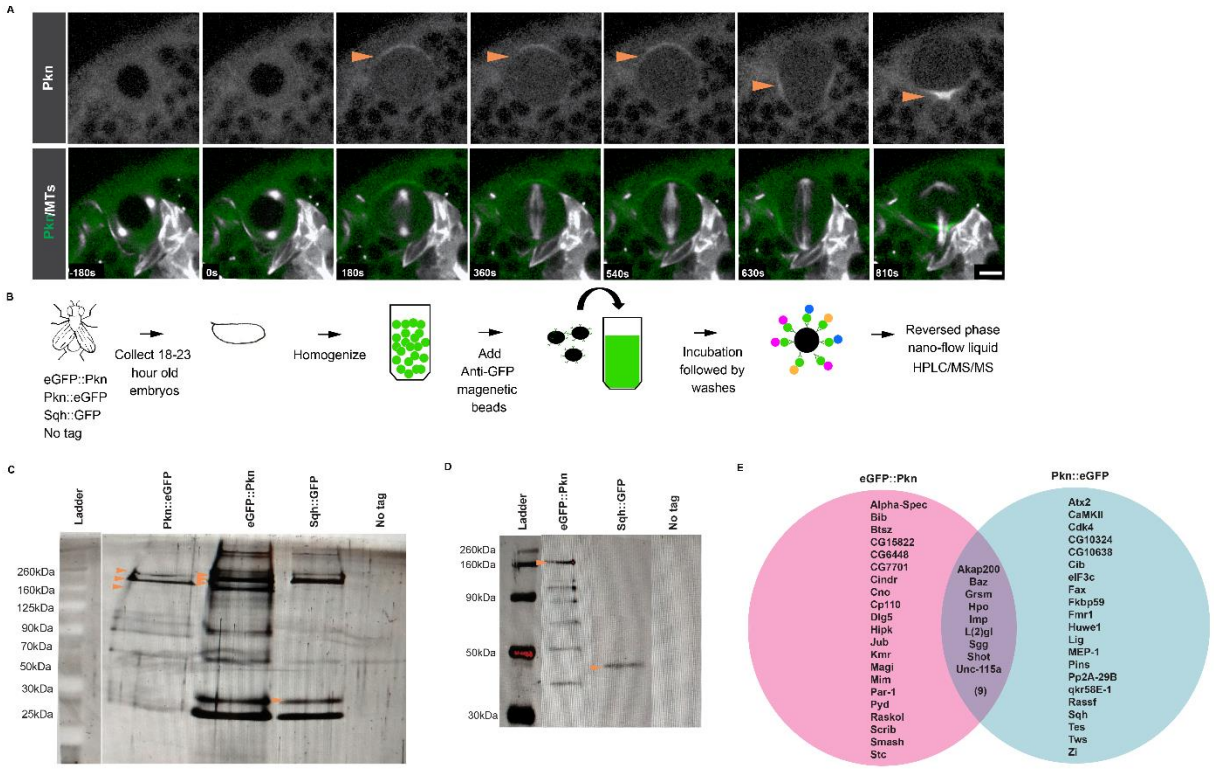

Figure 2: Identification of Pkn's Potential Binding Partners
A. Representative image sequence of Protein Kinase N (Pkn) CRISPR line third instar neuroblasts expressing Pkn::eGFP and mCherry::Jupiter (microtubules; MTs). Scale bar 5um. Time 0s is set to NEB. Orange arrow represents Pkn localization. **B.** Schematic representation of workflow. Embryonic pull-downs were conducted on 18-23 hour old embryos expressing eGFP::Pkn, Pkn::eGFP, Sqh::EGFP or no tag (*w;IF/CyO;MKRS/TM6B*). Then reversed phase nano-flow liquid HPLC/MS/MS was run on the elutions. Sample carryover was removed before analyzing MS results. The top candidates for both Pkn lines were selected based on molecular function, subcellular localization as well as conserved hits from human Co-IP STRING data. **C.** SYPRO Ruby stained SDS-PAGE gel on 10% elutions from anti-GFP pull-downs using 18-23 hour old embryos expressing eGFP::Pkn, Pkn::eGFP, Sqh::EGFP or no tag (*w;IF/CyO;MKRS/TM6B*). Orange arrow represents bands of interest suspected to be full-length eGFP::Pkn, Pkn::eGFP or Sqh::EGFP. **D.** Anti-GFP western blot on anti-GFP pull-down elutions using 18-23 hour old embryos expressing eGFP::Pkn, Pkn::eGFP, Sqh::EGFP or no tag (*w;IF/CyO;MKRS/TM6B*). Orange arrow represents full-length eGFP::Pkn or Sqh::EGFP. **E.** Venn diagram containing the top 30 candidates from eGFP::Pkn and Pkn::eGFP pull-downs.

Pkn diffuses universally in the cytoplasm until the subsequent mitosis where it becomes locally concentrated to the apical cortex during early metaphase (Figure 2A). In addition, our Pkn

CRISPR line as well as *Pkn*^{CC01654} are homozygous viable and fertile illustrating that the GFP insertion is not detrimental to development and/or Pkn's essential roles.

Once Pkn's dynamics were confirmed, Pkn anti-GFP pull-downs were conducted. Three grams of 18-23 hour old *Drosophila* embryos from C-terminally and N-terminally eGFP tagged Pkn flies, C-terminally eGFP tagged Sqh flies and non-GFP tagged flies were collected, the supernatants were used as bait for anti-GFP pull-downs followed by mass spectrometry on the pull-down elutions (Figure 2B). Based on our SYPRO Ruby stained SDS-PAGE gel, our pull-down elutions show numerous proteins are present, including proteins expected to be Pkn isoforms based on their molecular weight (eGFP::Pkn= 156-190kDa; Pkn::eGFP= 187-220kDa; Sqh::GFP= 48kDa) (Figure 2C). To confirm that Pkn was indeed pulled down, an anti-GFP western blot on our pull-down elutions shows an isoform of Pkn present (Figure 2D). We noted multiple bands present that are smaller than full length Pkn isoforms. Based on Pkn's sequence and utilizing the software PeptideCutter, Pkn has a potential cleavage site for Caspase 1 which can account for bands observed at 65kDa as well as 62kDa (Figure 2D).

After curating the mass spectrometry data centered on molecular function and subcellular localization, provided on UniportKB and FlyBase, as well as detecting conserved hits from published human Co-IP STRING data, over 50 potential binding partners of Pkn were identified [73–75]. Most of these candidates are subcellularly localized to the cell membrane, cytoskeleton and cytosol (Table 1 & Table 2). Their known molecular functions range from protein binding, kinase activity, ion binding and RNA binding (Table 1 & Table 2). Of these 60 candidates, 9 were identified in pull-downs from both Pkn fly lines (Figure 2E). Since kinases are known to quickly act on their perspective substrates, we suspect the differences in top candidates for these lines may be due to the substrate populations readily near Pkn during pull-down incubation.

Initial Characterization of Pkn's Potential Binding Partners

From the list of Pkn's top candidate binding partners, we choose to characterize 5 interesting candidates via RNA interference (RNAi) based on their molecular function and subcellular localization in *Drosophila* and/or vertebrates: *a kinase anchor protein 200* (*akap200*) (no human ortholog), *alpha spectrin* (human SPTAN1), *polychaetoid* (*pyd*) (human TJP2), s*haggy* (s*gg*) (human GSK3B) and *twins* (*tws*) (human PPP2R2D). Neuroblasts from these knockdowns were assessed for changes in Myosin dynamics associated to the polarity-dependent pathway to alter normal Myosin localization. If these proteins are involved in this pathway, we hypothesized that they would have a similar phenotype as observed in *pkn* mutants.

In one of the *a kinase anchor protein 200* (*akap200*) RNAi lines had abnormal apical Myosin enrichment as seen in our *pkn* mutant phenotype (Figure 3 & Table 3). While observing *alpha spectrin*, only 1 of 2 RNAi line resulted in rare occurrences of slightly higher Myosin apical enrichment (Figure 3 & Table 3). Additionally, neither *pyd* RNAi lines showed any defects in Myosin localization (0/130 neuroblasts) (Figure 3 & Table 3). As for *twins* (*tws*), in 2 of the 3 RNAi lines examined higher apical enrichment of Myosin was observed (Figure 3 & Table 3). While examining *shaggy* (*sgg*) RNAi lines, all lines had numerous neuroblasts with abnormal apical Myosin enrichment, similar to *pkn* mutant neuroblasts (Figure 4A & Table 3). We conclude *sgg* is a top candidate which based on multiple RNAi lines analysis alters Myosin dynamics. Based on the severity of this phenotype, we chose to verify this with the *sgg* mutant allele sgg^{1}. Unexpectedly, a phenotype was not observed in this mutant (Figure 4B). We suspect this may be due to this line being listed as both a hypomorphic as well as an amorphic allele. We plan to examine additional *sgg* alleles and assess for alterations to Myosin's proper spatiotemporal dynamics in the future. Previously published *Drosophila* neuroblast research has

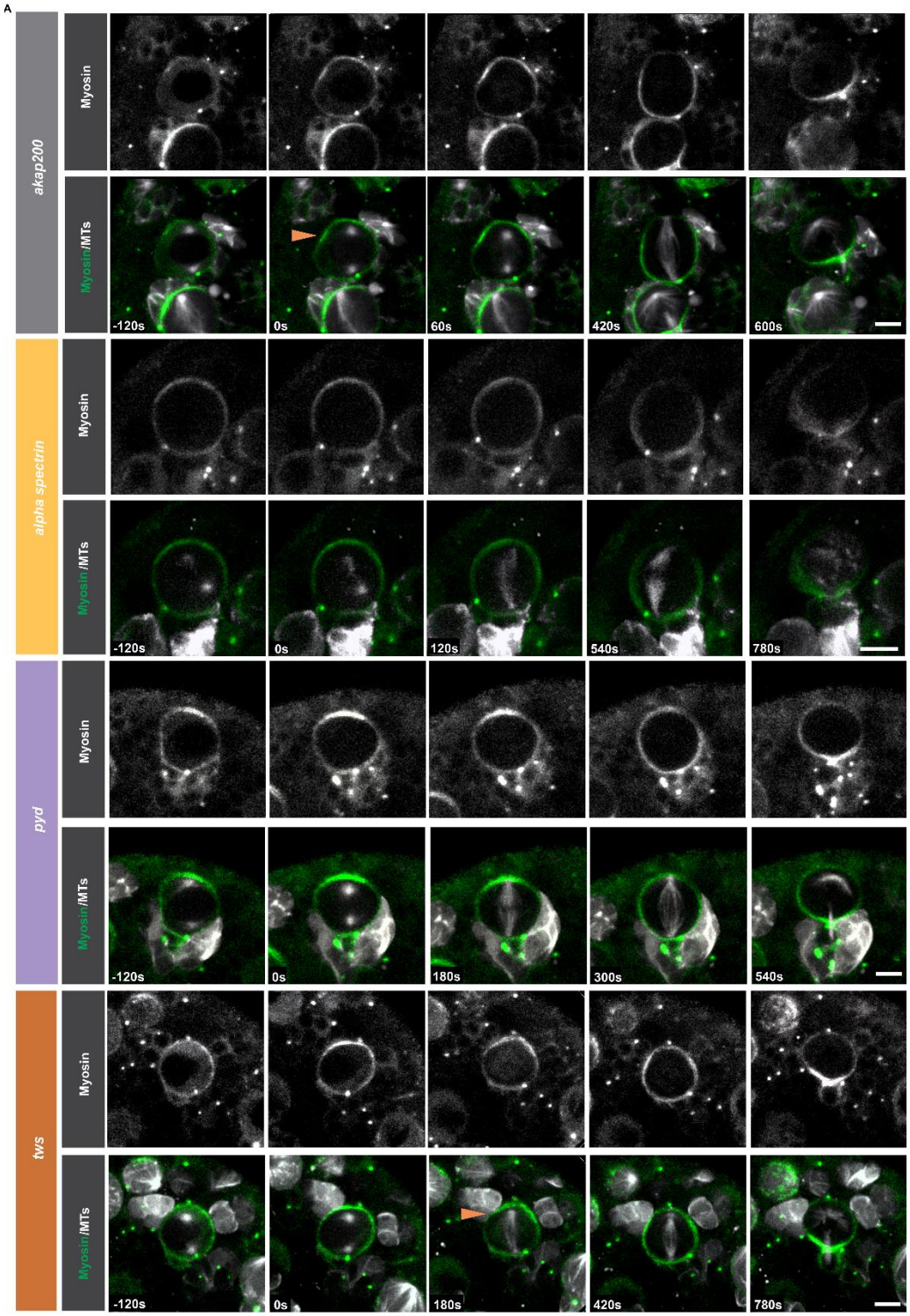

Figure 3: Initial Characterization of Pkn's Potential Binding Partners
Representative image sequence of a *kinase anchor protein 200* (*akap200*), *alpha spectrin*, *polychaetoid* (*pyd*), and t*wins* (*tws*) RNAi lines third instar neuroblast expressing Sqh::GFP (Myosin) and mCherry::Jupiter (microtubules; MTs). Scale bar 4um. Time 0s is set to NEB. Orange arrow represents apical Myosin enrichment.

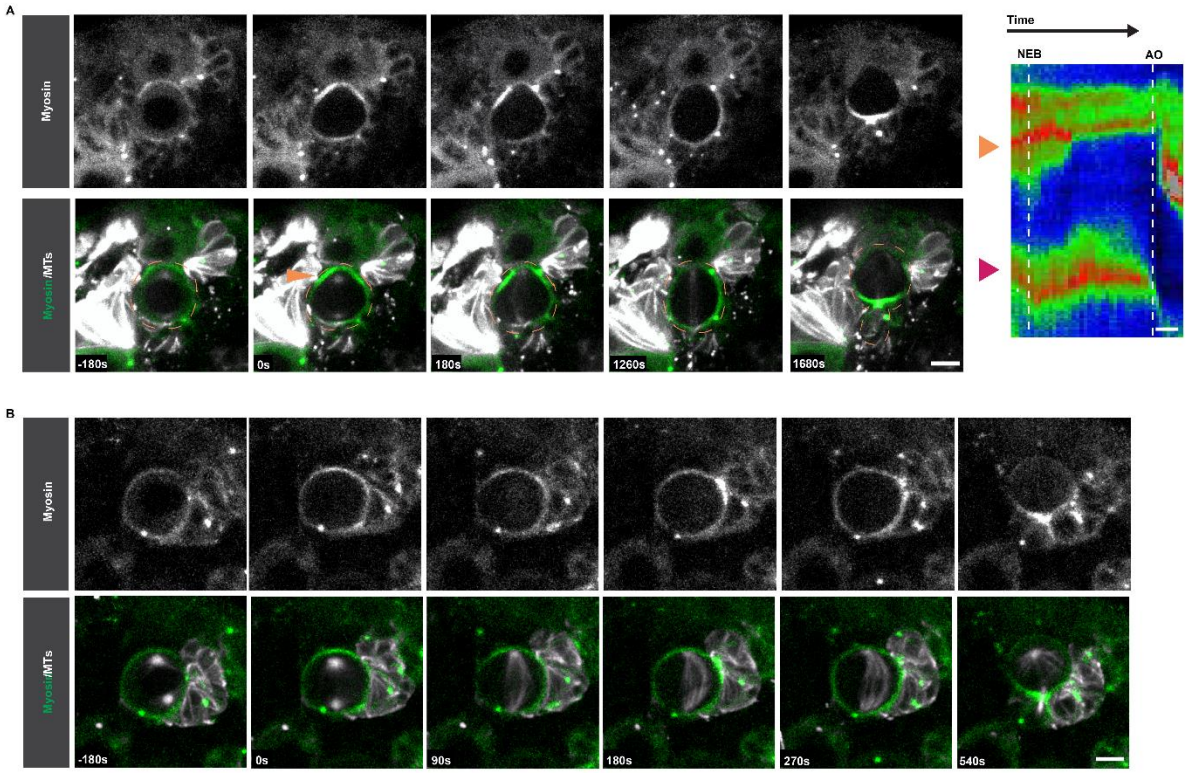

Figure 4: Initial Characterization of Pkn's Potential Binding Partner Shaggy
A. Representative image sequence of *shaggy* (*sgg*) RNAi line third instar neuroblasts expressing Sqh::GFP (Myosin) and Cherry::Jupiter (microtubules; MTs). Orange dashes circle around neuroblast through mitosis in dual channel panel. Orange arrow represents apical Myosin enrichment. Representative kymograph made along the apical to basal cortex. Arrowheads highlight the apical (orange) and the basal (magenta) cortex, respectively. The vertical dashed lines refer to the nuclear envelope breakdown (NEB) and anaphase onset (AO). 4 pixels/min scale bar. Intensity ranges are indicated by Rainbow LUT. **B.** Representative image sequence of *shaggy* mutant (sgg^{1}) third instar neuroblasts expressing Sqh::GFP (Myosin) and mCherry::Jupiter (microtubules; MTs). Scale bar 4um. Time 0s is set to NEB.

found Lethal Giant Larvae (Lgl) (Human LLGL1) interacts with Myosin's heavy chain (Zipper) (human MYH10) and at least one other actin-associated protein while in an unphosphorylated state [76]. In neuroblasts, *lgl* mutants have been shown to undergo symmetric as well as inverted divisions [77]. This inversion phenotype is similar to that of *pkn* mutants. Moreover, Lgl is known to be phosphorylated by the Serine/Threonine Kinase aPKC (human PRKCI) resulting in conformational change in Lgl thus inhibiting it from associating with the cell cortex [76].

Since Lgl was a candidate from our mass spectrometry data, we wondered whether Pkn could also phosphorylate Lgl and indirectly alter Myosin localization. Before beginning any genetic characterization, live cell imaging on third instar larvae was conducted and Lgl dynamics, via an an endogenous mCherry tagged Lgl line, alongside Pkn dynamics, via our Pkn::eGFP CRISPR line, were examined in neuroblasts (Supplemental Figure 1). Unfortunately, data utilizing this Lgl protein trap line was inconclusive as Lgl was found to only localized to some cell junctions. This is counter to previously published immunohistochemistry staining, utilizing an anti-Lgl antibody, which have shown Lgl to be localized to the apical cortex of neuroblasts during the early stages of mitosis [77].

Myosin Trapping Results in Altered Physical Asymmetry

To assess whether alterations to sibling cell size can lead to differences in cell fate, we altered sibling cell size via a nanobody approach. Active Myosin, via myosin regulatory light chain called Squash (Sqh), was permanently trapped to the apical cortex of neuroblasts using an anti-GFP nanobody (vhhGFP) [78]. The nanobody was fused to an apical localizing domain and driven by a neuroblast specific Gal4 driver, *worniu* [16]. Consistent with previous results [16], apical Myosin trapping can induce altered physical asymmetry (Figure 5A). Since prior published research has established the typical wildtype neuroblast as well as Ganglion Mother Cell sizes and our wildtype data aligns, we chose to define the upper threshold of normal ACD based on this data (2.39) [16,79]. To define the cutoff for symmetric sibling cell size ratio, the wildtype neuroblast cell size distribution was utilized to determine the cutoff of normal ACD. Since wildtype neuroblasts always had a ratio greater than 1.6. Thus, this can be reliably used as the upper threshold of SCD. Additionally, a ratio of 1.0 was selected for the lower cell size threshold as symmetric cells will have this ratio. Hence any cell size ratio between 1.6-1.0 was

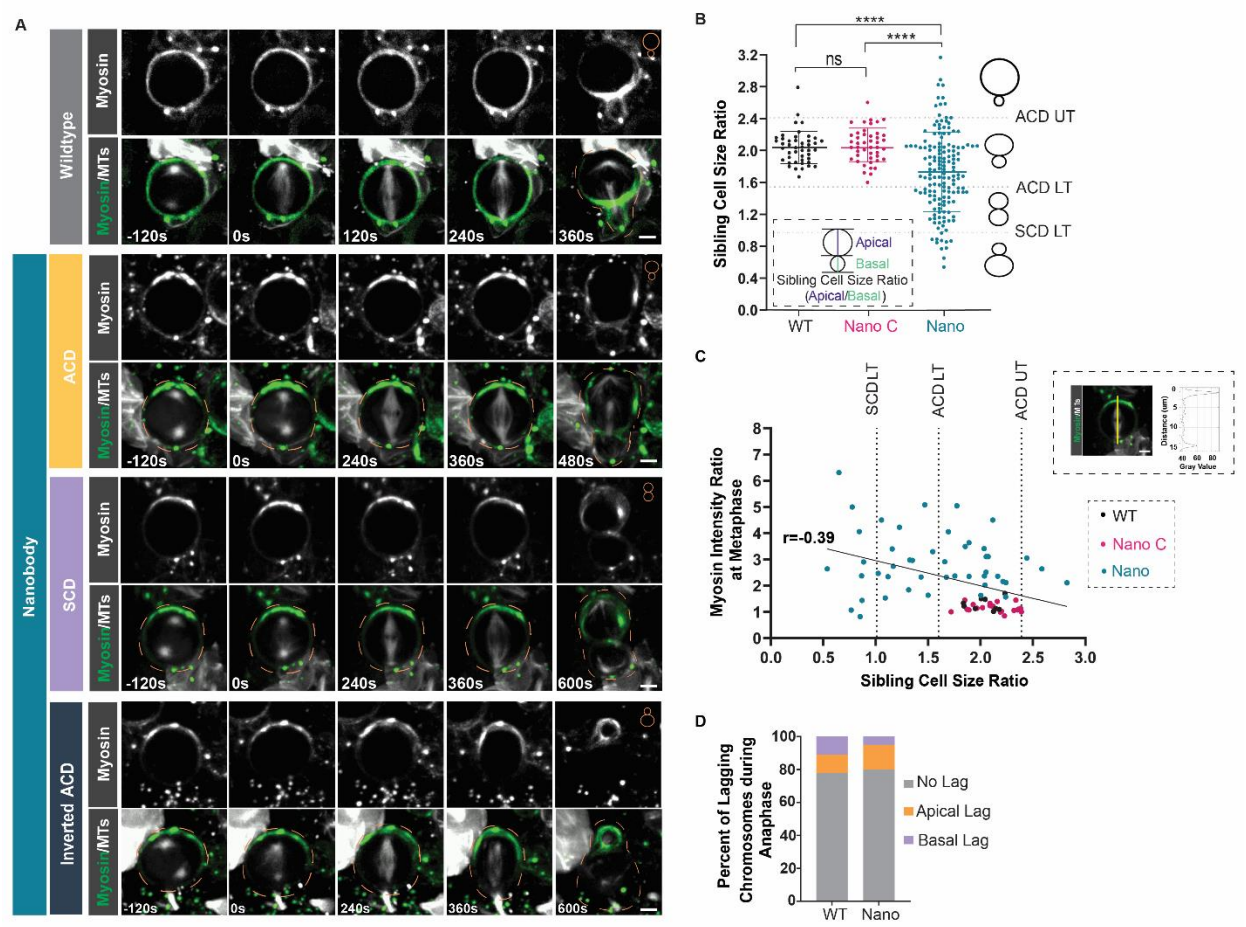

Figure 5: Myosin Trapping Results in Altered Physical Asymmetry

A. Representative image sequences of wildtype and Squash nanobody expressing third instar neuroblasts. Scale bar 4um. Time 0s is set to NEB. Inverted ACD= Inverted Asymmetric Cell Division, SCD= Symmetric Cell Division, MTs= microtubules. Orange dashes circle around selected neuroblast through mitosis in dual channel panel. **B.** Scatter plot of sibling cell size ratios of wild type, nanobody control and Squash nanobody expressing neuroblast. Each dot represents a neuroblast sibling cell size ratio. Mean and standard deviation plotted. WT= Wildtype, Nano C= Nanobody Control, Nano= Nanobody, UT= Upper Threshold, LT= Lower Threshold, Normal ACD sibling cell size ratio = 2.3-1.6, Normal SCD sibling cell size ratio= 1.6-1.0, Normal Inverted ACD sibling cell size ratio = <1.0. **C.** Representative image of wildtype third instar neuroblast in metaphase expressing Sqh::GFP (Myosin) and Cherry::Jupiter (microtubules; MTs). Yellow line represents Myosin intensity value (gray value) obtained from apical cortex to basal cortex by drawing a line through the cortexes using the spindle as a marker. Scatter plot of Myosin intensity value of wildtype, nanobody control and Squash nanobody expressing neuroblasts at metaphase plotted against their corresponding for sibling cell size ratio. A linear regression was plotted, and significance was determined by Spearman's coefficient. WT= Wildtype, Nano C= Nanobody Control, Nano= Nanobody. **D.** Bar graph showing the number of lagging chromosomes observed at telophase during live cell imaging wildtype and Squash nanobody expressing third instar neuroblast expressing Sqh::GFP (Myosin) and His2A::RFP. Apical Lag= apical cell chromosomes lag, Basal Lag= basal cell chromosomes lag.

Figure 5 Continued: Myosin Trapping Results in Altered Physical Asymmetry
D. WT= Wildtype, Nano= Nanobody.

categorized as symmetric. As for inverted asymmetric sibling cell size ratio, any value below 1.0 was categorized as such. We found the sibling cell size ratio of nanobody expressing cells were significantly different from wildtype and nanobody control neuroblasts (Figure 5B).

Based on the results, we wondered whether the amount of Myosin trapped on the apical cortex during metaphase is correlated with subsequent sibling cell size. To assess this, Myosin's intensity ratio was obtained from nanobody expressing as well as wildtype, nanobody control neuroblasts during metaphase and were plotted against their resulting sibling cell size ratio (Figure 5C). A weak negative correlation, r=-0.39, was observed (Figure 5C). Thus, a higher Myosin intensity ratio at metaphase is weakly correlated with a smaller sibling cell size.

Due to changes in sibling cell size asymmetry via the nanobody approach, we wanted to assess whether alterations in chromosome separation occur. Live cell imaging on third instar larvae was conducted and nanobody expressing cells as well as wildtype neuroblasts were examined for lagging chromosomes during anaphase via Histone 2A, His2A::RFP. No significant difference in the number of lagging chromosomes between wildtype neuroblasts and nanobody expressing cells were observed (Figure 5D). In conclusion, Myosin trapping can alter physical asymmetry without affecting chromosome separation and this asymmetry is weakly correlated with the amount of Myosin located on the apical cortex during metaphase.

Global Changes in Physical Asymmetry Alter Cell Cycle Timing

One method to assess alterations in cell fate is by measuring changes in cell cycle timing. We chose to conduct 6-9 hour live cell imaging sessions on intact larval brains in order to track individual neuroblasts and their lineages. Since previous research has found wildtype neuroblast

divide once every 60-90 minutes and Ganglion Mother Cells divide every 8-10 hours, this information was used to assess possible changes in cell fate [79,80].

As previously reported, wildtype neuroblasts divided with a cell cycle timing of 117 +/- 43.4 minutes and Ganglion Mother Cells did not divide during the imaging sessions (Figure 6A, 6B & 6D) [79]. In nanobody expressing brains, apical cells underwent asymmetric, symmetric and inverted asymmetric divisions (Figure 6C). In inverted asymmetric sibling cell lineages, most sibling cells did not undergo division (Figure 6A, 6B & 6D).

Additionally, small apical cells generated by inverted ACD did not divide (Figure 6A & 6G). We speculate there may be a cell size threshold which if not met may result in apoptosis. In symmetric sibling cell lineages, the majority of sibling cells did not divide again (Figure 6A, 6C & 6F). Based on our nanobody expressing sibling cell lineages, we wondered in total how many basal sibling cells underwent subsequent division. Only basal sibling cells resulting from symmetric and inverted asymmetric divisions were found to divide again (Figure 6A, 6E, 6F & 6G).

To understand the connection between cell size and cell cycle timing, we assessed how many apical and basal sibling cells divide generated during symmetric as well inverted asymmetric divisions. Of those symmetric divisions, 6 apical cells divided again with a cell cycle length of 125 +/- 63.6 minutes while 3 basal cells divided again with a cell cycle of 265+/- 273 minutes (Figure 6F). In contrast, 1 large basal cell generated from inverted asymmetric division divided again and had a cell cycle timing of 180 minutes (Figure 6G). Together, we conclude global changes in physical asymmetry affect cell cycle timing of the resulting sibling cells and therefore promote alterations to cell fate.

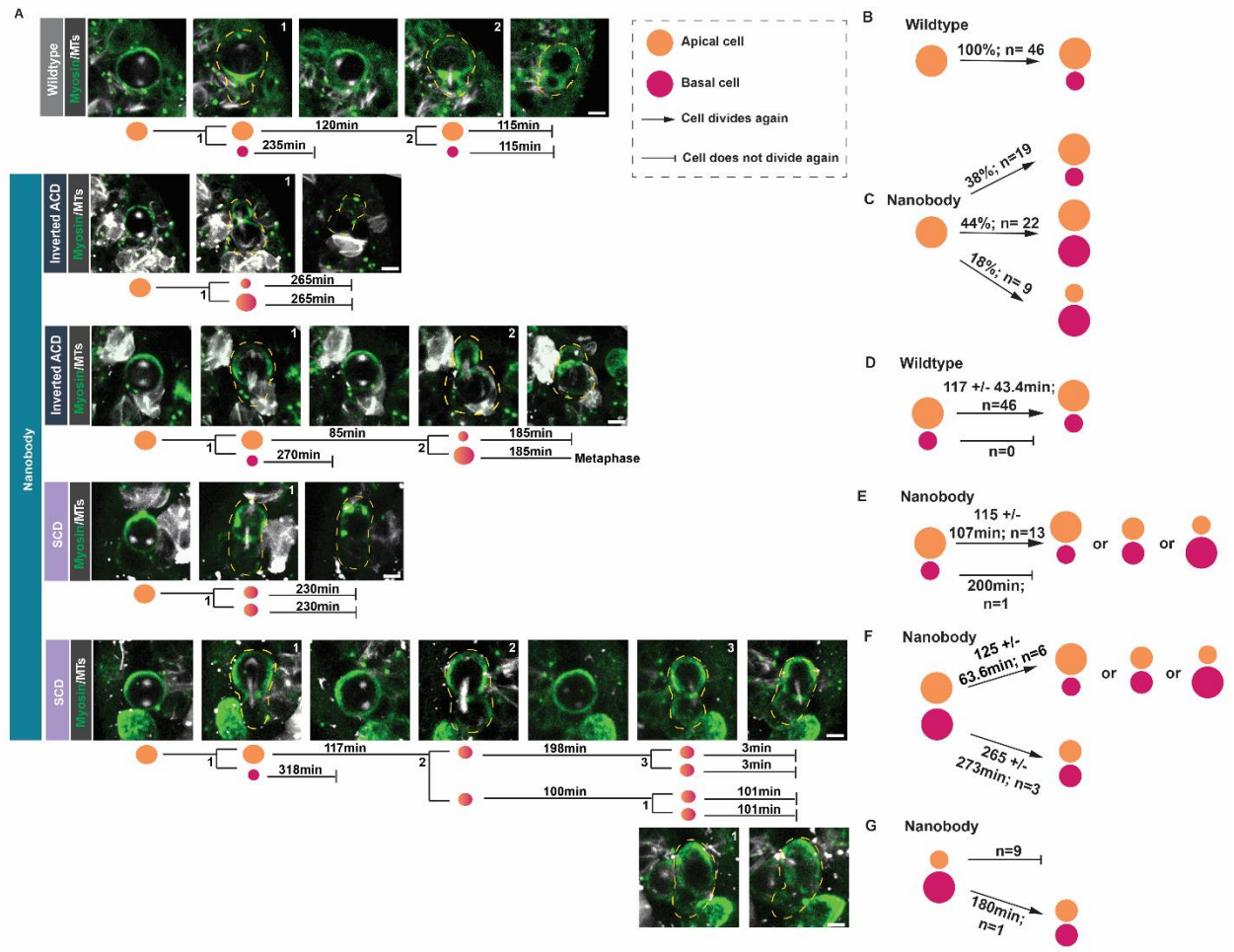

Figure 6: Global Changes in Physical Asymmetry Alters Cell Cycle Timing
A. Representative image sequences of individual wildtype and Squash nanobody third instar neuroblasts lineage trees from 6-9 hour live cell imaging sessions on larval brains. Cell cycle timing of the daughter cells were calculated from telophase to prophase along with sibling cell size ratio. Scale bar 4um. Time 0min is set to beginning of movie. MTs= microtubules. Yellow dashes circle around selected neuroblast at telophase. **B.** Diagram illustrating the percent of wildtype third instar neuroblasts observed with the following division pattern during the live cell imagining sessions. n= individual neuroblasts. **C.** Diagram illustrating the percent of Squash nanobody third instar apical cells observed with the following division pattern during the live cell imagining sessions. n= individual apical cells. **D.** Diagram illustrating the average cell cycle timing of wildtype third instar neuroblasts and Ganglion Mother Cells with the following division pattern during the live cell imagining sessions. n= individual neuroblasts. Mean cell cycle timing and standard deviation listed. **E.** Diagram illustrating the average cell cycle timing of Squash nanobody third instar apical and basal cells resulting from an asymmetric cell division during the live cell imagining sessions. n= individual neuroblasts. Mean cell cycle timing and standard deviation listed. **F.** Diagram illustrating the average cell cycle timing of Squash nanobody third instar apical and basal cells resulting from a symmetric cell division during the live cell imagining sessions. n= individual neuroblasts. Mean cell cycle timing and standard

Figure 6 Continued: Global Changes in Physical Asymmetry Alters Cell Cycle Timing deviation listed. **G.** Diagram illustrating the average cell cycle timing of Squash nanobody third instar apical and basal cells resulting from an inverted asymmetric cell division during the live cell imagining sessions. n= individual neuroblasts. Mean cell cycle timing and standard deviation listed.

Global Changes in Physical Asymmetry Alters the Nuclear Size and Number of Neuroblasts

To provide additional support for changes to cell fate due to altered cell size, changes in cell fate marker expression in control and nanobody expressing third instar brains were examined via immunohistochemistry. Since wildtype neuroblast always express the neuroblast fate transcription factor Deadpan (human HES1) and Ganglion Mother Cells always express nuclear Prospero (human PROX1), a differentiated fate transcription factor, these markers were selected for our experiments [81–83]. We noticed nanobody expressing larval brains had fewer as well as smaller Deadpan positive nuclei than control brains (Figure 7A). Quantifying the number of Deadpan positive nuclei in the central brains of nanobody expressing and control larvae, significantly fewer Deadpan positive cells were present in nanobody expressing larval brains (Figure 7B). Additionally, the mean size of Deadpan positive nuclei in nanobody expressing central brains was significantly smaller (Figure 7C & 7D). To determine whether the diameter of Prospero positive nuclei in the central brains of nanobody expressing and control were different, their size was quantified, and no significant difference was observed (Figure 7E & 7F).

Since the size of Deadpan positive nuclei in nanobody expressing nuclei was significantly smaller and looked comparable to the nuclear size of wildtype Prospero positive Ganglion Mother Cell nuclei, we chose to compare their nuclear diameters. Based on our analysis, there was a significant difference between nanobody expressing Deadpan positive nuclei and wildtype Prospero positive Ganglion Mother Cell nuclei (Figure 7G). Although there is a significant

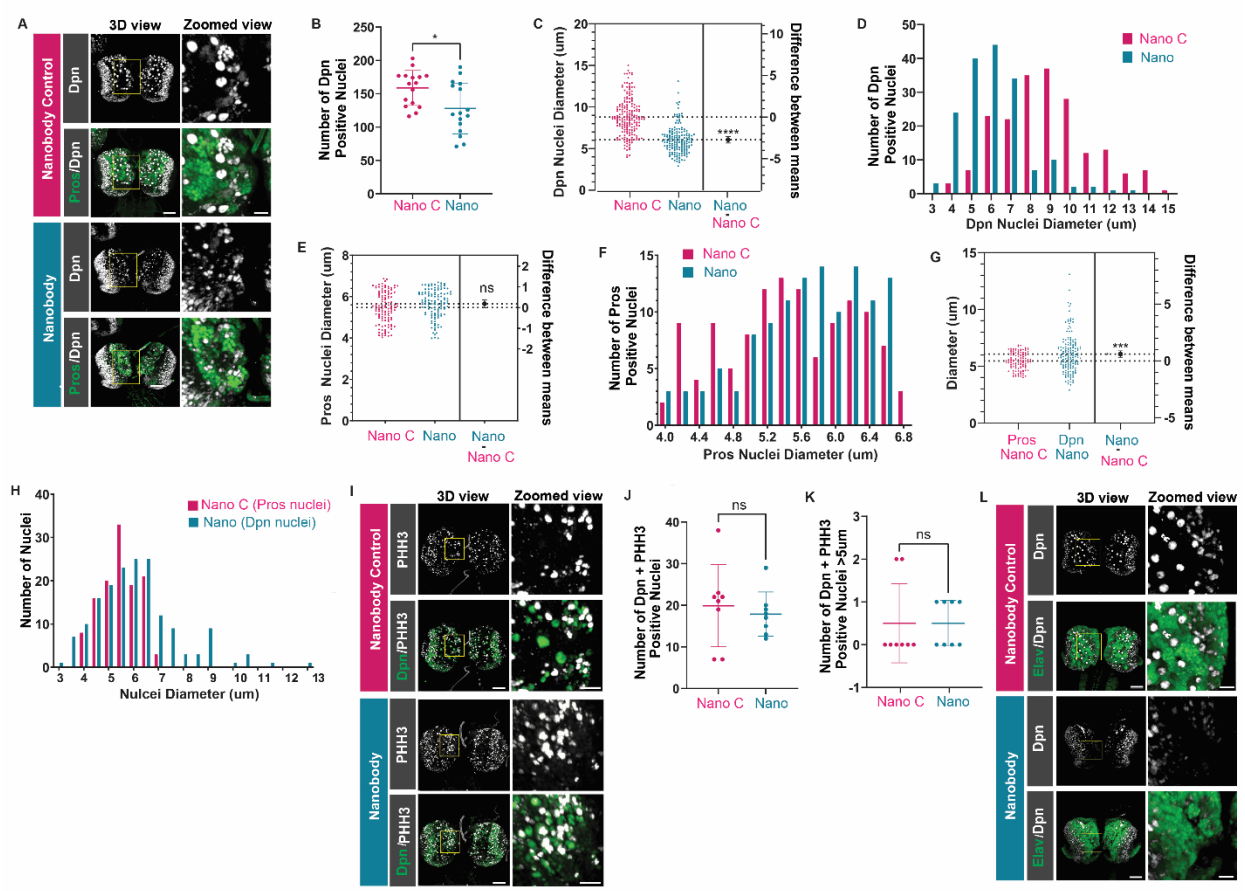

Figure 7: Global Changes in Physical Asymmetry Alters the Nuclear Size and Number of Postulated Neuroblasts

A. Representative images of nanobody control and Squash nanobody expressing larval brains fixed and stained for Deadpan and Prospero. Yellow rectangles represent region selected for zoomed view. Scale bar is 50um for 3D view and 20um for zoomed view. Nano C= Nanobody Control, Nano= Nanobody, Dpn= Deadpan, Pros= Prospero. **B.** Scatter plot of Deadpan positive nuclei from nanobody control and Squash nanobody expressing larval brain lobes. Each dot represents the number of Deadpan positive cells in a single central brain lobe. Mean and standard deviation plotted. **C.** Estimation plot of Deadpan positive nuclear diameter from nanobody control and Squash nanobody expressing larval brains. **D.** Distribution of Deadpan positive nuclear diameter collected in panel C. **E.** Estimation plot of Prospero positive nuclear diameter from nanobody control and Squash nanobody expressing larval brains. **F.** Distribution of Prospero positive nuclear diameter collected in panel E. **G.** Estimation plot of Prospero positive nuclear diameter from nanobody control and Deadpan positive nuclear diameter from Squash nanobody expressing larval brains. **H.** Distribution of Prospero positive nuclear diameter from nanobody control and Deadpan positive nuclear diameter from Squash nanobody expressing larval brains collected in panels C and E. **I.** Representative images of nanobody control and Squash nanobody expressing larval brains fixed and stained for Deadpan and Phosphorylated Histone H3. Yellow rectangles represent region selected for zoomed view. Scale bar is 50um for 3D view and 20um for zoomed view. Nano C= Nanobody Control, Nano= Nanobody, Dpn= Deadpan, PHH3= Phosphorylated Histone H3. **J.** Scatter plot of Deadpan and Phosphorylated

Figure 7 Continued: Global Changes in Physical Asymmetry Alters the Nuclear Size and Number of Postulated Neuroblasts
J. Histone H3 dual positive nuclei from nanobody control and Squash nanobody expressing larval brains. Each dot represents the number of dual positive nuclei within a single central brain lobe. Mean and standard deviation plotted.
K. Scatter plot of Deadpan and Phosphorylated Histone H3 dual positive nuclei less than 5um in size from nanobody control and Squash nanobody expressing larval brains. Each dot represents the number of dual positive nuclei >5um within a single central brain lobe. Mean and standard deviation plotted. **L.** Representative images of nanobody control and Squash nanobody expressing larval brains fixed and stained for Deadpan and Embryonic Lethal Abnormal Vision. Yellow rectangles represent region selected for zoomed view. Scale bar is 50um for 3D view and 20um for zoomed view. Nano C= Nanobody Control, Nano= Nanobody, Dpn= Deadpan, Elav= Embryonic Lethal Abnormal Vision.

difference, a majority of nanobody expressing Deadpan positive nuclei binned with wildtype Prospero positive Ganglion Mother Cell nuclei (Figure 7H). In conclusion, the majority of Deadpan positive nuclei from nanobody expressing brains are similar in size to Prospero positive cells suggesting that they may have arisen from inverted divisions.

To examine whether the expression changes caused by alterations in physical asymmetry could affect proliferation, immunohistochemistry was conducted on control and nanobody expressing third instar brains using the proliferation marker Phosphorylated Histone H3 (PHH3) alongside Deadpan. No statistical significance in the number of dual positive cells, Deadpan and PHH3, between control and nanobody expressing brains was observed (Figure 7I). We suspect this is likely due to the maintained population of Mature Intermediate Neural Progenitors in Type II neuroblast lineages. These cells are known to express Deadpan, be mitotically active and lack the expression of *worniu* so they do not exhibit Myosin trapping. Additionally, the few Deadpan positive nuclei less than 5um which were also PHH3 positive had no observable differences (Figure 7K). Thus, Deadpan positive nuclei in nanobody expressing brains exhibit similar proliferation patterns seen in control brains.

Based on these results, we wondered whether changes to sibling cell size could result in

abnormal neuronal development. Immunohistochemistry was conducted on control and nanobody expressing third instar brains using the neuronal marker Embryonic Lethal Abnormal Vision (Elav) (human ELAVL2) and Deadpan. No observable changes to neuronal development were detected in nanobody expressing brains (Figure 7L) [84]. We speculate that a sizable population must undergo symmetric and inverted asymmetric cell division to observe abnormal neuronal development. In conclusion, global changes in sibling cell size asymmetry alter cell cycle timing as well as number and nuclear size of cells postulated to have a neuroblast fate.

Retention of the Scaffolding Protein Miranda Alters Cell Fate

Based on our inverted physical asymmetry cell cycle timing results, we wondered whether inverting molecular ACD could also result in altered cell fate. Previous research has utilized the misalignment of the mitotic spindle orientation, orthogonal to apical/basal polarity, in *Drosophila* neuroblasts to alter cell determinants [79]. They found the ratio of apical to basal determinants can specify neuroblasts and Ganglion Mother Cell identity [79]. Additionally, the proteins required to shuttle basal fate determinants are well known in *Drosophila* neuroblasts [55,85]. Specifically, the scaffolding protein, Miranda (human SLMAP), is known to directly bind Prospero as well as Brain Tumor (human TRIM3), two basal fate determinants, and shuttle them into the Ganglion Mother Cell [86–89]. Although there is another basal cell fate determinant, Numb (human NUMBL), it is not shuttled by Miranda but instead by Partner of Numb (human ST6GAL1) [89–91]. Together, these basal fate determinants inhibit transcription and translation of stemness related genes resulting in the commitment to neuronal differentiation.

Utilizing this information, we wondered whether permanently trapping Miranda would alter the localization of basal fate determinants. Thus, the nanobody approach was used to permanently trap endogenously eGFP tagged Miranda to the apical cortex in neuroblasts and

assess whether this is sufficient to alter cell fate. Since homozygous eGFP tagged Miranda flies are not viable, Miranda was trapped in heterozygous background. In nanobody expressing neuroblasts, a portion of Miranda was trapped to the apical cortex while some continued to segregate basally (Figure 8A). Additionally, we found a subset of Prospero was trapped to the apical cortex while also localizing basally (Figure 8B). In nanobody expressing cells, no alterations to the distribution of the basal cell fate determinant Numb was observed (Figure 8B). Thus, although a portion of Miranda and Prospero are trapped apically, other basal fate determinants such as Numbs' localization, remains unaltered and polarity is nevertheless maintained.

To determine if the amount of trapped Miranda could alter cell fate, sibling cells were examined for changes in cell cycle timing. A significant increase in apical cell cycle timing was observed in nanobody expressing brains (Figure 8C & 8D). No adjustments in cell cycle timing were detected in the basal sibling cells (no data shown). We hypothesize that the wide distribution in cell cycle timing is most likely due to differences in the amount of trapped Miranda and Prospero in individual cells. Therefore, the ratio of apical to basal determinants in each apical sibling cell will vary. In conclusion, global changes in molecular asymmetry affect apical cell cycle timing and therefore promote alterations to cell fate.

To provide further support for altered cell fate due to changes in the ratio of apical to basal determinants, changes in cell fate marker expression in control and nanobody expressing third instar brains were assessed via immunohistochemistry. In the central brain region of nanobody expressing brains, the number of Deadpan positive nuclei was significantly higher (Figure 8E & 8F). Additionally, the mean size of Deadpan positive nuclei in nanobody expressing central

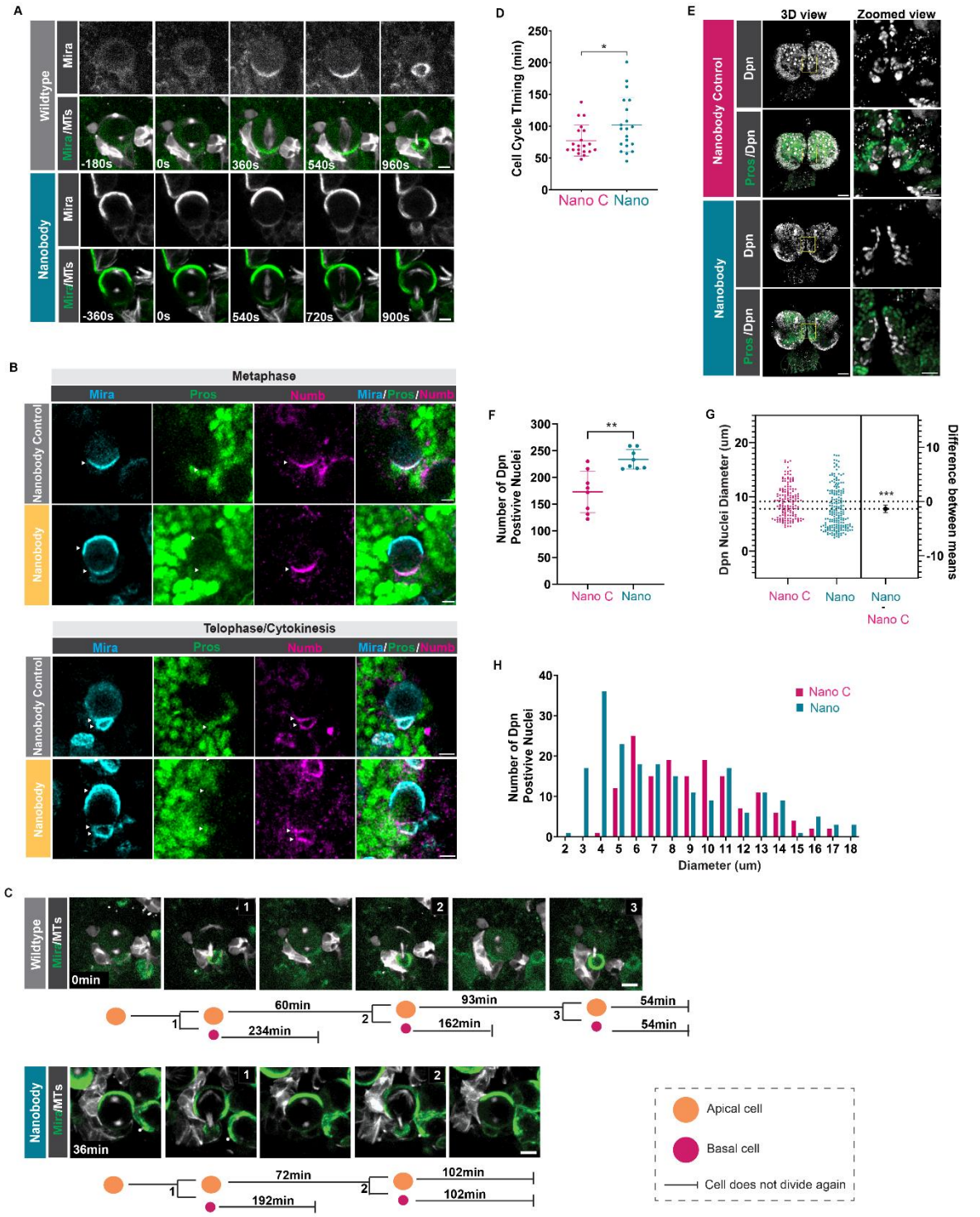

Figure 8: Retention of the Scaffolding Protein Miranda Alters Cell Fate

A. Representative image sequences of wildtype and Miranda nanobody expressing third instar neuroblasts. Scale bar 4um. Time 0s is set to NEB. Mira= Miranda, MTs= microtubules.

B. Representative neuroblasts in metaphase and telophase/cytokinesis of nanobody control and Miranda nanobody expressing larval brains fixed and stained for Prospero and Numb.

Figure 8 Continued: Retention of the Scaffolding Protein Miranda Alters Cell Fate
B. White arrows represent localization of protein. Scale bar 5um. Mira= Miranda, Pros= Prospero. **C.** Representative image sequences of wildtype and Miranda nanobody third instar neuroblasts lineages from 6-9 hour live cell imaging sessions on larval brains. Cell cycle timing of the daughter cells were calculated from telophase to prophase along with sibling cell size ratio. Scale bar 4um. Time 0min is set to beginning of movie. Mira= Miranda, MTs= microtubules, NB= neuroblast. **D.** Scatter plot of cell cycle timing data for nanobody control and Miranda nanobody expressing neuroblast. Each dot represents a single neuroblast/apical cell. Mean and standard deviation plotted. Cell cycle timing of the apical daughter cell was calculated from telophase to prophase. Nano C= Nanobody Control, Nano= Nanobody. **E.** Representative image of nanobody control and Miranda nanobody expressing larval brains fixed and stained for Deadpan and Prospero. Yellow rectangles represent region selected for zoomed view. Scale bar is 50um for 3D view and 20um for zoomed view. Nano C= Nanobody Control, Nano= Nanobody, Dpn= Deadpan, Pros= Prospero. **F.** Scatter plot of Deadpan positive nuclei from nanobody control and Miranda nanobody expressing larval brain lobes. Each dot represents a central brain lobe. Mean and standard deviation plotted. **G.** Estimation plot of Deadpan positive nuclear diameter from nanobody control and Miranda nanobody expressing larval brains. **H.** Distribution of Deadpan positive nuclear diameter collected in panel G.

brains was significantly spread compared to control central brains (Figure 8F & 8G). Specifically, the size of the Deadpan positive nuclei in nanobody expressing central brains ranged from those smaller than that of wildtype Prospero positive Ganglion Mother Cell nuclei to larger than that of Deadpan positive wildtype neuroblast nuclei (Figure 8H). In conclusion, retention of the scaffolding protein Miranda alters cell fate via changing the ratio of basal fate determinants which segregate into the sibling cells as well as the number of cells and the nuclear size of cells postulated to have a neuroblast fate.

Discussion

Here we have identified over 50 potential binding partners of Pkn. Based on initial RNAi characterization Sgg, and Tws as well as published Lgl data, altered Myosin dynamics similar to *pkn* mutant phenotypes were observed. We propose Lgl, Sgg and/or Tws may directly interact with Pkn to control Myosin's spatiotemporal dynamics during *Drosophila* neuroblast division

[77]. Further research is needed to determine whether these proteins directly bind to Pkn, and if so, whether they are upstream or downstream of Pkn.

For instance, in *Drosophila*, Lgl has been reported to be phosphorylated by aPKC at 3 different Serine residues (656, 660, 664) [92–94]. We hypothesize Pkn may also phosphorylate Lgl to further remove any remaining interaction with Myosin's heavy chain, thus indirectly disturbing Myosin's localization on the apical cortex. Based on *Drosophila's* Pkn sequence, it is highly conserved with human Pkn 1, human Pkn 2 and human Pkn 3. Since the consensus motif of *Drosophila* Pkn's kinase domain is not known, we wondered whether it resembles the consensus motif of human Pkn 1 and/or human Pkn 3 [95]. If so, we would suspect to observed this the consensus motif in *Drosophila* Lgl. Based on our sequence examination, we infer *Drosophila* Lgl is recognized by human Pkn 1 as well as human Pkn 3 at S656. Therefore, future research should be conducted to determine whether *Drosophila* Pkn phosphorylates *Drosophila* Lgl at this site.

We have demonstrated that alterations in physical as well as molecular asymmetry affect cell fate observed by changes in cell cycle timing as well as the number and nuclear size of cells postulated to have a neuroblast fate. We propose these alterations in cell fate may have long term developmental consequences. As previously mentioned, in *C. elegans*, altering spindle positioning via LIN-5 during the first embryonic division can result in lineage defects including cell cycle timing, cell positioning, division axis as well as apoptosis [62]. We suspect that, like *C. elegans*, there may be a sibling cell size threshold requirement in order to maintain viability. For instance, the small Deadpan positive nuclei in Myosin nanobody expressing brains in our experiments most likely arose from an inverted division. We hypothesize there could be a cell size threshold which once reached, cells may undergo apoptosis. Additional research should be

conducted to determine whether there is a cell size threshold and the consequences of surpassing it.

Our research has found that alterations in sibling cell size via global trapping Myosin to the apical cortex of neuroblasts throughout the developing brain is sufficient to alter cell fate. To gain a clearer picture of this process, future research should be conducted to alter sibling cells in a more specific manner. For instance, by trapping Myosin in a single neuroblast or a small subset of neuroblasts, consequences resulting from an inverted division such as cell fate and lineage positioning can be easily assessed. We propose trapping Myosin to the apical cortex in Type 1 neuroblasts via the well characterized Gal-4 driver Ase [96], and assessing for changes to cell fate will be enlightening.

To our knowledge, inverted molecular asymmetry by the mislocalization of a scaffolding protein, thus altering basal fate determinants, has not been reported in flies, humans, mice or worms. Previous research in *Drosophila* has found the ratio of apical to basal determinants determines neuroblast and Ganglion Mother Cell fate via cell cycle timing as well as cell fate markers [79]. To gain a deeper understanding of the requirements behind ACD maintenance studies should be conducted to alter the location of single as well as multiple basal fate determinants.

Overall, our research has begun to elucidate the mechanisms and functions of ACD in *Drosophila* neuroblasts. Since not much is known about Pkn, it is our hope that our research spurs interest in identifying the molecules involved in establishing asymmetry in this system. Whether these findings are conserved in other organisms that undergo ACD remains to be seen.

Table 1: Mass Spectrometry Hits for eGFP::Pkn (Fly Line 247)								
Protein Name	**PSM (single isoform example)**	**Listed in human Co-IP PMID: 31046837?**	**Listed in human Co-IP from PMID: 25702638?**	**Molecular Function-1**	**Molecular Function-2**	**Molecular Function-3**	**Subcellular Location**	**Signaling Pathway**
Alpha-Spec	954	Y	N	actin binding	calmodulin binding	calcium ion binding	cytoskeleton	None Listed
Shot	568	Y	Y	actin binding	microtubule binding	calcium ion binding	cytoskeleton	None Listed
Kmr	451	N	N	regulation of establishment of planar polarity	phosphatidylinositol bisphosphate binding		plasma membrane	None Listed
Baz	227	N	N	phosphatidylinositol binding			plasma membrane	None Listed
Smash	225	N	N	metal ion binding			cell junctions	None Listed
Cindr	210	N	N	SH3 domain binding			plasma membrane (cleavage furrow), midbody, intercellular bridge	None Listed

Table 1: Mass Spectrometry Hits for eGFP::Pkn (Fly Line 247)								
Protein Name	**PSM (single isoform example)**	**Listed in human Co-IP PMID: 31046837?**	**Listed in human Co-IP from PMID: 25702638?**	**Molecular Function-1**	**Molecular Function-2**	**Molecular Function-3**	**Subcellular Location**	**Signaling Pathway**
Magi	208	N	N	small GTPase binding			plasma membrane	None Listed
Unc-115a	200	N	N	actin binding	metal ion binding		cytoskeleton	None Listed
Pyd	192	N	Y	protein binding	cell adhesion molecule binding		plasma membrane, axon, adherent junctions	Positive Regulators of Hippo
Cno	112	N	N	protein binding	ATP binding	small GTPase binding	plasma membrane, adherent junctions, cell cortex	None Listed
Raskol	94	N	N	GTPase activator activity			cytoplasm, cell membrane	None Listed

Table 1: Mass Spectrometry Hits for eGFP::Pkn (Fly Line 247)								
Protein Name	**PSM (single isoform example)**	**Listed in human Co-IP PMID: 31046837?**	**Listed in human Co-IP from PMID: 25702638?**	**Molecular Function-1**	**Molecular Function-2**	**Molecular Function-3**	**Subcellular Location**	**Signaling Pathway**
Jub	79	N	N	metal ion binding	protein sequestering activity	transcriptional corepressor activity	adherent junctions	Negative Regulators of Hippo
L(2)gl	46	N	N	GTPase activator activity	syntaxin binding	myosin binding	cortex	Negative Regulators of Notch; Positive Regulators of Hippo
CG7701	40	X	X	unknown			unknown	None Listed

Table 1: Mass Spectrometry Hits for eGFP::Pkn (Fly Line 247)								
Protein Name	**PSM (single isoform example)**	**Listed in human Co-IP PMID: 31046837?**	**Listed in human Co-IP from PMID: 25702638?**	**Molecular Function-1**	**Molecular Function-2**	**Molecular Function-3**	**Subcellular Location**	**Signaling Pathway**
Scrib	38	Y	N	protein binding			cell membrane, cytoplasm, tight junctions	None Listed
CG6448	33	N	N	protein phosphatase 1 binding			cell membrane	None Listed
Mim	29	N	N	actin binding	phospholipid binding	protein homodimerization activity	cytoskeleton	None Listed
CG15822	29	N	N	phosphatidylinositol binding			cell membrane	None Listed
Cp110	26	N	N	None listed			centriole	None Listed

Table 1: Mass Spectrometry Hits for eGFP::Pkn (Fly Line 247)								
Protein Name	**PSM (single isoform example)**	**Listed in human Co-IP PMID: 31046837?**	**Listed in human Co-IP from PMID: 25702638?**	**Molecular Function-1**	**Molecular Function-2**	**Molecular Function-3**	**Subcellular Location**	**Signaling Pathway**
Akap200	22	NA	NA	actin binding	Notch binding		cell membrane, cytoskeleton, cytosol	Positive Regulators of Notch
Grsm	21	N	N	manganese ion binding	metalloaminopeptidase activity		cytoplasm	None Listed
Hpo	20	N	N	protein kinase activity	ATP binding		cytoplasm, plasma membrane	Hippo
Bib	18	N	N	ion channel activity	water transmembrane transporter activity		plasma membrane	None Listed
Dlg5	18	N	N	None listed			plasma membrane	Negative Regulators of Hippo
Stc	15	N	N	Zinc ion binding	DNA-binding transcription factor activity	RNA binding	nucleus	None Listed

Table 1: Mass Spectrometry Hits for eGFP::Pkn (Fly Line 247)								
Protein Name	**PSM (single isoform example)**	**Listed in human Co-IP PMID: 31046837?**	**Listed in human Co-IP from PMID: 25702638?**	**Molecular Function-1**	**Molecular Function-2**	**Molecular Function-3**	**Subcellular Location**	**Signaling Pathway**
Hipk	14	N	N	DNA binding	beta-catenin binding		cytosol, nucleus	Positive Regulators of Wnt-TCF; Negative and Positive Regulators of Hippo; Positive Regulators of Hedgehog; Positive Regulators of Notch
Sgg	11	Y	N	protein kinase activity			cytosol, centrosome, mitotic spindle, plasma	Negative Regulators of Wnt-TCF; Negative

Table 1: Mass Spectrometry Hits for eGFP::Pkn (Fly Line 247)								
Protein Name	**PSM (single isoform example)**	**Listed in human Co-IP PMID: 31046837?**	**Listed in human Co-IP from PMID: 25702638?**	**Molecular Function-1**	**Molecular Function-2**	**Molecular Function-3**	**Subcellular Location**	**Signaling Pathway**
							membrane, nucleus	Regulators of Insulin-like Receptor; Negative Regulators of Hedgehog
Par-1	6	Y	N	protein serine/threonine kinase activity	ATP binding		cytosol, plasma membrane, fusome	Negative Regulators of Hippo
Imp	5	Y	Y	RNA binding			cytosol, nucleus, axon, cytoplasm	Positive Regulators of JAK-STAT

Table 2: Mass Spectrometry Hits for Pkn::eGFP (Fly Line MD15)								
Protein Name	**PSM (single isoform example)**	**Listed in human Co-IP PMID:31046837?**	**Listed in human Co-IP from PMID:25702638?**	**Molecular Function-1**	**Molecular Function-2**	**Molecular Function-3**	**Subcellular Location**	**Signaling Pathway**
Sqh	67	N	N	calcium ion binding			cytoskeleton	None Listed
Zi	19	Y	Y	cytoskeletal motor activity			cytoskeleton	None Listed
Pins	18	N	N	GTPase regulatory activity			cortex	None Listed
Baz	1	N	N	Phosphatidylinositol binding			plasma membrane	None Listed
L(2)gl	1	N	N	GTPase activator activity	myosin binding		cortex	Negative Regulators of Notch; Positive Regulators of Hippo
Hpo	117	N	N	protein kinase activity			cytoplasm, plasma membrane	Hippo
Rassf	181	N	N	metal ion binding			cytosol	Negative Regulators of Hippo

Table 2: Mass Spectrometry Hits for Pkn::eGFP (Fly Line MD15)								
Protein Name	**PSM (single isoform example)**	**Listed in human Co-IP PMID:31046837?**	**Listed in human Co-IP from PMID:25702638?**	**Molecular Function-1**	**Molecular Function-2**	**Molecular Function-3**	**Subcellular Location**	**Signaling Pathway**
MEP-1	43	N	N	DNA-binding transcription factor activity			nucleoplasm, nucleus	None Listed
Imp	10	Y	Y	RNA binding			cytosol, nucleus, axon, cytoplasm	Positive Regulators of JAK-STAT
Atx2	35	Y	N	RNA binding			cytoplasm	None Listed
Huwe1	31	Y	N	ubiquitin protein ligase activity			nucleus, cytoplasm	Negative Regulators of Wnt-TCF; Negative Regulators of TNFα-Eiger
CG10638	30	NA	NA	transketolase activity			cytosol	None Listed
Fkbp59	28	Y	N	peptidyl-prolyl cis-trans			cytoplasm	None Listed

Table 2: Mass Spectrometry Hits for Pkn::eGFP (Fly Line MD15)								
Protein Name	**PSM (single isoform example)**	**Listed in human Co-IP PMID:31046837?**	**Listed in human Co-IP from PMID:25702638?**	**Molecular Function-1**	**Molecular Function-2**	**Molecular Function-3**	**Subcellular Location**	**Signaling Pathway**
				isomerase activity				
Grsm	19	N	N	metal ion binding			cytoplasm	None Listed
Lig	9	Y	N	actin binding	microtubule binding	calcium ion binding	cytoskeleton	None Listed
CG10324	2	N	N	protein binding			cytoplasm	Negative Regulators of JAK-STAT; Positive Regulators of Hippo
Fmr1	11	Y	Y	unknown			nucleus	None Listed
Tws	10	Y	N	RNA binding			cytoplasm, neuron projection, synapse, stress granule	Negative Regulators of Insulin-like Receptor

Table 2: Mass Spectrometry Hits for Pkn::eGFP (Fly Line MD15)								
Protein Name	**PSM (single isoform example)**	**Listed in human Co-IP PMID:31046837?**	**Listed in human Co-IP from PMID:25702638?**	**Molecular Function-1**	**Molecular Function-2**	**Molecular Function-3**	**Subcellular Location**	**Signaling Pathway**
Pp2A-29B	2	N	N	protein phosphatase regulator activity			cytoplasm, nucleus	Positive Regulators of Hedgehog; Positive Regulators of Wnt-TCF
Tes	1	Y	N	protein phosphatase regulator activity			centriole, cytosol, nucleoplasm	Negative Regulators of Insulin-like Receptor; Negative Regulators of Hippo; Negative Regulators of Hedgehog
Shot	1	Y	Y	metal ion binding			cytoskeleton , cytoplasm	None Listed
Cib	5	N	N	actin binding			cytoskeleton	None Listed
Fax	4	N	N	protein			plasma	None Listed

Table 2: Mass Spectrometry Hits for Pkn::eGFP (Fly Line MD15)								
Protein Name	**PSM (single isoform example)**	**Listed in human Co-IP PMID:31046837?**	**Listed in human Co-IP from PMID:25702638?**	**Molecular Function-1**	**Molecular Function-2**	**Molecular Function-3**	**Subcellular Location**	**Signaling Pathway**
				binding			membrane, cytoplasm	
Cdk4	6	Y	Y	protein kinase activity			nucleus	Positive Regulators of JAK-STAT
CaMKII	5	N	N	protein kinase activity			postsynaptic membrane, axon, cytoplasm, neuron projection	None Listed
qkr58E-1	3	Y	Y	mRNA binding			nucleus	None Listed
Akap200	3	NA	NA	actin binding	Notch binding		cell membrane, cytoskeleton, cytosol	Positive Regulators of Notch
eIF3c	2	Y	N	translation initiation factor activity			cytoplasm	None Listed
Unc-115a	2	N	N	actin binding	metal ion binding		cytoskeleton	None Listed

Table 2: Mass Spectrometry Hits for Pkn::eGFP (Fly Line MD15)								
Protein Name	**PSM (single isoform example)**	**Listed in human Co-IP PMID:31046837?**	**Listed in human Co-IP from PMID:25702638?**	**Molecular Function-1**	**Molecular Function-2**	**Molecular Function-3**	**Subcellular Location**	**Signaling Pathway**
Sgg	1	Y	N	protein kinase activity			cytosol, centrosome, mitotic spindle, plasma membrane, nucleus	Negative Regulators of Wnt-TCF; Negative Regulators of Insulin-like Receptor; Negative Regulators of Hedgehog

Table 3: Initial Characterization of Pkn's Potential Binding Partners			
Gene	**Bloomington Stock Number**	**Phenotype(s) observed in RNAi expressing neuroblasts**	**Number of neuroblasts with phenotype**
akap200	28532	Apical Myosin enrichment, bent spindle	1/70
alpha spectrin	31209	None	0/70
alpha spectrin	42801	Apical Myosin enrichment, bent spindle, larger cells	0/70
pyd	28920	None	0/60
pyd	35335	None	0/70
sgg	35364	Apical Myosin enrichment, blebbing	6/80
sgg	31308	Apical Myosin enrichment, multiple active centrosomes, spindle realignment	15/50
sgg	31309	Apical Myosin enrichment	4/80
tws	38899	Multiple active centrosomes, spindle realignment	7/70
tws	28714	Apical Myosin enrichment, blebbing, larger cells	9/60
tws	36689	Apical Myosin enrichment, blebbing, spindle realignment, larger cells	4/60

Supplemental Figure

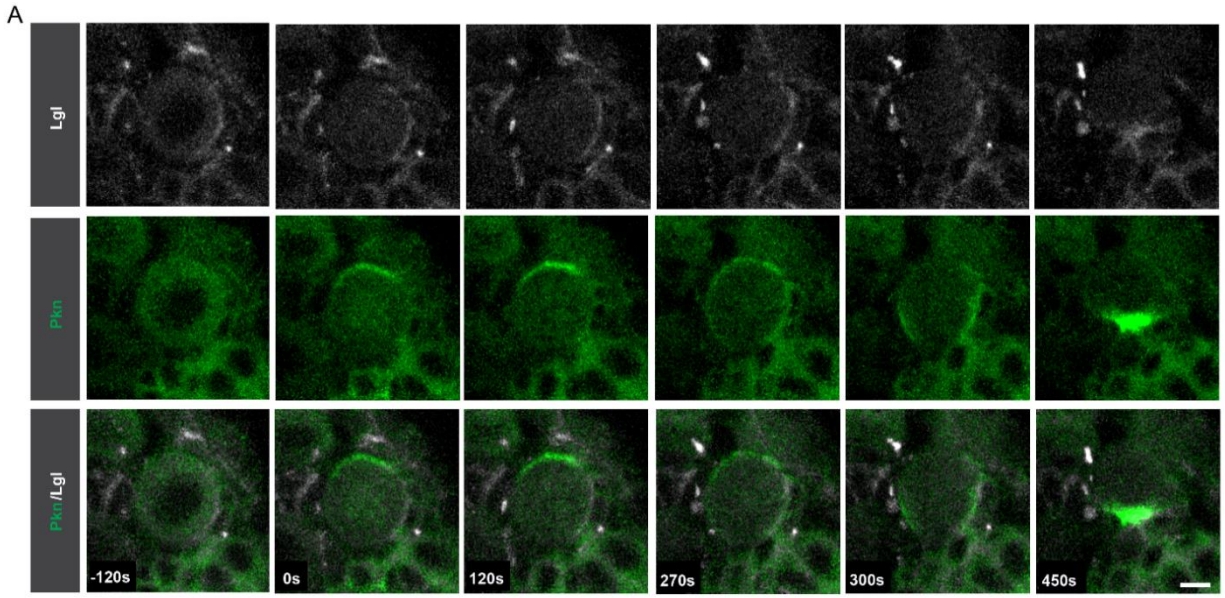

Supplemental Figure 1

A. Representative image sequence of wildtype third instar neuroblasts expressing Lgl::mCherry (Lethal Giant Larvae) and Pkn::eGFP (Protein Kinase N). Scale bar 4um. Time 0s is set to metaphase.

Methods

Fly lines: The following fly lines were used in this publication.

Fly Lines		
Stock Number	**Genotype**	**Notes**
MD10	*w; worGal4,UAS-mcherry::Jupiter/CyO; UAS-ALDInscuteable RockKinase domain-VhhGFP-HA/TM6B*	
MD15	*w; Pkn::eGFP::SSPB/CyO; MKRS/TM6B*	CRISPR line
MD64	*w; FRT 42B pkn 1T/ CyOActGFP;TM6B/MKRS*	Balanced line from the Martinho lab
MD76	*w; Pkn06736/CyOActGFP; worGal4, UAS-mCherry::Jupiter, Sqh::EGFP/TM6B*	
MD114	*w-; ALD_insc::Vhh::HA,worGal4,UAS-mCherry::Jupiter/CyO;MKRS/TM6B*	
MD122	*w; worgal4, His2A::RFP (#4)/CyO; UAS ALDInscuteable RockKinase domain-VhhGFP-HA/TM6B*	
MD126	*Sqh::eGFP::SSPB/y x Sqh::eGFP::SSPB/FM7C*	CRISPR line
MD142	*w; FRT 42B pkn 1T/ CyOActGFP;worGal4,UAS-mcherry::Jupiter, Sqh::eGFP/TM6B*	
MD137	*w; Df(2R)w73-1/CyOActGFP; worGal4,UAS-mCherry::Jupiter, Sqh::eGFP/TM6B*	
MD156	*w; IF/CyO; Mira::eGFP/TM6B*	Mira::eGFP line generated by D. Salvador-Garcia using CRISPR
MD166	*w-; worGal4,mCherry::Jupiter/CyO; Mira::eGFP/TM6B*	
MD169	*w; UAS-mcherry::Jupiter, Sqh::eGFP/CyO;UAS-ALDInscuteable RockKinase domain-VhhGFP4-HA/TM6B*	
Lab stock 144	*w; Sqh::GFP,worGal4,UAS-mcherry::Jupiter/CyO; Dr/TM6B*	
Lab stock 247	*w; eGFP::Pkn(CC01654)/(CyO); MKRS/TM6B*	Protein Trap (GFP) line originally from BDSC 51566
Lab stock 308	*w; IF/CyO; UAS-ALDInscuteable RockKinase domain-VhhGFP-HA/TM6B*	
Lab stock 760	*w; Pkn06736/CyOactGFP; MKRS/TM6B*	

Fly Lines- Continued		
Stock Number	**Genotype**	**Notes**
Lab stock 728	*w; IF/CyO; MKRS/TM6B*	
AM146	*Sqh-;Sqh::GFP/CyO; MKRS/TM6B*	
BDSC 851	*y[1] w[67c23] P{y[+mDint2]=Crey}1b; D[*]/TM3, Sb[1]*	
BDSC 4095	*sgg[1]/FM7a/Dp(1;2;Y)w[+]*	*sgg* mutant
BDSC 36289	*l(2)gl[4] P{ry[+t7.2]=neoFRT}40A/CyO*	*l(2)gl4* mutant
BDSC 41561	*w[*]; l(2)gl[27S3] P{ry[+t7.2]=neoFRT}40A/CyO*	*l(2)gl27S3* mutant
BDSC 31209	*y1 v1; P{TRiP.JF01727}attP2*	Alpha Spectrin
BDSC 42801	*y1 v1; P{TRiP.GL01173}attP2*	Alpha Spectrin
BDSC 38899	*y1 v1; P{TRiP.GL00670}attP40/CyO*	Tws
BDSC 28714	*y1 v1; P{TRiP.JF03141}attP2/TM3, Sb1*	Tws
BDSC 36689	*y1 sc* v1 sev21; P{TRiP.HMS01578}attP2*	Tws
BDSC 28532	*y1 v1; P{TRiP.HM05018}attP2*	Akap200
BDSC 35364	*y[1] sc[*] v[1] sev[21]; P{y[+t7.7] v[+t1.8]=TRiP.GL00277}attP2*	Sgg
BDSC 31308	*y[1] v[1]; P{y[+t7.7] v[+t1.8]=TRiP.JF01255}attP2*	Sgg
BDSC 31309	*y[1] v[1]; P{y[+t7.7] v[+t1.8]=TRiP.JF01256}attP2/TM3, Ser[1]*	Sgg
BDSC 28920	*y1 v1; P{TRiP.HM05131}attP2*	Pyd
BDSC 35225	*y[1] sc[*] v[1] sev[21]; P{y[+t7.7] v[+t1.8]=TRiP.GL00109}attP2*	Pyd
Dr. Lee's lab	*Lgl-mCherry FP217 (II)*	Protein trap line

Pkn CRISPR line generation: The following web tools were used to design target specific sequences with high efficiency:

CRISPR Optimal Target Finder (http://tools.flycrispr.molbio.wisc.edu/targetFinder/), DRSC CRISPR finder (http://www.flyrnai.org/crispr/) and Efficiency Predictor (http://www.flyrnai.org/evaluateCrispr/). Sense and antisense primers for these chosen sites were then cloned into pU6-BbsI-ChiRNA between BbsI sites (Gratz et al., 2013).

Target Site 1: Sense: GAAGCAGGTGGAATTCGTTAGAAATTGAATAATAATCTGTT

Target Site 1: Anti-Sense: CTTGCTCACGCGGCCGCACACCATTCGGCCGTGTATGAA

Target Site 2: Sense: GCACTAGTAAAGATCTTAGAAGCTCATTCTTAGTTCAAGGATTTA CTAACGGGCCTAGAA

Target Site 2: Anti-Sense: ACGGAAGAGCCTCGAGTCCAAATTCTATCCCGTCGAG

The replacement donor template SSPB (Addgene #60416) as well as EGFP and 1kb homology arms flanking the insertion site were cloned into pHD-DsRed-attP (Addgene plasmid #51019) using Takara's Infusion technology [97]. Best Gene injected embryos for pHD-Pkn::EGFP::SSPB-DsRed along with the replacement donor plasmid and its corresponding pU6-BbsI-ChiRNA (www.thebestgene.com). Once fly lines were obtained from Best Gene, they were screened for DsRed. To remove the DsRed, the F1 progeny we crossed to a constitutively active Cre line. The proper progeny was then balanced, genotyped and sequenced.

Anti-GFP based Protein Purification and Liquid Chromatography/Mass Spectrometry Analysis:

Protein purification: A rabbit anti-GFP antibody kindly gifted by Dr. Alexey Merz was coupled to M-270 Epoxy dynabeads (Co-Immunoprecipitation Kit Thermo 14321D). 18-23 hour old embryos expressing eGFP::Pkn, Pkn::eGFP, Sqh::EGP or no tag (w;IF/CyO;MKRS/TM6B) were collected on grape juice plates. To collect sufficient number of embryos, multiple collections occurred where the processed and kept at -80C until pull-downs were completed. These embryos were then washed and dechorionated. After dechorionation, embryos were washed 3x with RNase/DNase/Protease free water, transferred to 1.5ml low protein binding microfuge tubes, weighed and immediately snap frozen in liquid nitrogen. Once 3mg of embryos of each genotype were obtained, pull-downs were conducted following the protocol provided

(Thermo 14321D) with a few modifications. PhosSTOP and cOmplete mini EDTA free protease inhibitor cocktail were added to the EB buffer (Roche 4906845001 and Roche 11836170001) Additionally, after 1 hour incubation of lysate with the antibody-coupled dynabeads, 2 washes of 200ul 1x LWB (+RapiGest SF, no triton) were performed. Additionally, 2 stepwise elutions were preformed 0.2M acetic acid then 1M ammonium hydroxide. Once elutions complete 10% were checked and estimated for efficiency by SYPRO Ruby stain (Thermo S12000). The remaining 90% was flash frozen in liquid nitrogen prior to sample preparation for mass spectrometry. Reactions were prepared for mass spectrometry (MS) analysis by drying in a speedvac at room temperature until dry. The acetic acid elution for each purification was resuspended by adding 15 uL of 50 mM ammonium bicarbonate and vortexing. Samples were sonicated in a water bath sonicator for 5 minutes, briefly centrifuged and the resulting resuspended protein was transferred into the tube containing the dried down ammonium hydroxide elution. These samples were then vortexed and sonicated as before resulting in a single tube containing both eluates. One uL of 1M ammonium bicarbonate was added to each tube to bring pH to 8. Samples were brought up to 0.1% rapigest (Waters Corporation) plus 5 mM TCEP and reduced for 60 mins at 60°C in an Eppendorf Thermomixer with shaking (1200 rpm). Alkylation was performed at room temperature in the dark for 30 mins with 6 mM iodoacetamide. Excess iodoacetamide was quenched by addition of 5 mM DTT and samples were then digested by trypsin digestion (Sequencing Grade Modified Trypsin, Promega Corp) at 37°C for 6 hours in a Thermomixer with shaking (1000 rpm) at a substrate to enzyme ratio of 15:1 prior to acidification with 250 mM HCl (final concentration). Acidified samples were incubated for 1 hour at room temperature, spun at max speed in a microfuge and supernatants containing peptides were transferred to autosampler vials and stored at -80°C until analysis.

Liquid Chromatography: For each sample injection onto the mass spectrometer, 3 µl of protein digests were loaded by autosampler onto a 150µm Kasil fritted trap packed with 2 cm of ReprosilPur C18AQ (3µm bead diameter, Dr. Maisch) at a flow rate of 2.5 µl/min. After desalting with 8 µl of 0.1% formic acid plus 2% acetonitrile, the trap was brought online with a Self-Packed PicoFrit Column (New Objective part number PF360-75-10-N-5, 75 µm i.d.) packed with 30 cm of Reprosil-Pur C18AQ (3µm bead diameter, Dr. Maisch) mounted to a heated nanospray ionization source (CorSolutions LLC) set at 50°C and placed in line with a Thermo Scientific EASY-nLC 1200 UPLC pump plus autosampler.

Peptides were eluted from the column at 0.25 µL/min using the following acetonitrile gradient: (1) 0-10 mins; 6-10% B; (2) 10-90 mins; 10-32% B; (3) 90-130 mins; 32-75% B; (4) 130-135 mins; 75% B; (5) 135-136 mins; 75-100% B; (6) 136-151 mins; 100% B, followed by re-equilibration to 5% buffer B prior to the subsequent injection. Buffer A was: 0.1% formic acid in water and buffer B was 0.1% formic acid 80% acetonitrile.

Data acquisition: A Thermo Fisher Scientific Exploris 480 was used to perform mass spectrometry in positive ion mode with the following settings. Data dependent acquisition (DDA) mode was used with a cycle time of 2 seconds between MS scans. MS spectra were acquired with a scan range of m/z 400–1,600. The resolution for MS and MS/MS was 60,000 and 15,000 at m/z 200, respectively. The normalized automatic gain control targets MS and MS/MS were set to 300% and 100%, respectively, and the maximum injection times were set to auto. MS/MS spectra were acquired using an isolation width of 2.5 m/z and a normalized collision energy of 27. MS/MS acquisitions were prevented for +1, +2, ≥+6 or undefined precursor charge states. Dynamic exclusion was set for 5 seconds. MS and MS/MS spectra were collected in centroid mode.

MS data processing – identification of proteins present in each sample: Raw mass spectra were converted into mzML using ProteoWizard's msconvert [98]. All proteins in each sample were identified using Comet version 2021.02 [99] searching against a database including the entire *Drosophila melanogaster* proteome (Uniprot Proteome ID UP000000803) plus common contaminants (https://www.thegpm.org/crap/) along with the sequences of all heterologously expressed proteins. The decoy database consisted of the corresponding set of reversed protein sequences. A statistically meaningful q-value was assigned to each peptide spectrum match (PSM) through analysis of the target and decoy PSM distributions using Percolator version 3.05 [100]. All data reported in this paper were filtered to show hits to the target proteins that had a Percolator assigned peptide level q value 0.01.

Mass spectrometry data analysis: Mass spectrometry was deposited and visualized on Limelight [75]. Raw data for each sample has been provided in the Supplements. Additionally, the raw data can be obtained here: https://limelight.yeastrc.org/limelight. Sample carryover was manually removed before analyzing MS results. The top 30 candidates for both Pkn lines were selected based on molecular function and subcellular localization listed on UniportKB and FlyBase as well as conserved hits from human Co-IP STRING data (Emani et al., 2015; J. H. Lee et al., 2019). Top hits were assembled and listed in Table 1 & Table 2.

SDS-PAGE: 10% elutions along with 10ul of Chameleon Duo Pre-stained ladder (LI-COR 928-60000) were ran on 10% resolving gels. Gels were then stained using SYPRO Ruby Protein Gel Stain (Thermo S12000). Gels were imaged on University of Washington's Biology Department shared ChemidocMP.

Anti-GFP Western Blot: Samples along with 10ul Chameleon 700 Pre-stained Protein Ladder (LI-COR 928-70000) were run on 10% resolving gels then transferred overnight at 4C onto a

PVDF membrane. Membrane was then blocked for 90 minutes in blotto (2% BSA + 1x TBS). The blot was then incubated overnight at 4C with primary antibody solution (Anti-GFP rabbit IgG Abcam ab6556 diluted 1:500 in 1xTBS). 3 washes of TBST (1x TBS + 0.1% tween-20) for 5 minutes were carried out. The blot was then incubated for 1 hour at room temperature with secondary antibody solution (Donkey anti-Rabbit IgG (H+L) Highly Cross-Adsorbed Secondary Antibody, Alexa Fluor Plus 647 Invitrogen A32795 diluted 1:1,000 in 1xTBS). 3 washes of TBST (1x TBS + 0.1% tween-20) for 5 minutes were carried out followed by 1 wash of TBS. Membranes were imaged on University of Washington's Biology Department shared ChemidocMP.

Immunohistochemistry: Third instar larval brains were dissected in S2 medium (Sigma-Aldrich S0146) and fixed for 20 min in 4% paraformaldehyde in PEM (100mM PIPES pH 6.9, 1mM EGTA and 1mM MgSO 4). After fixing, the brains were washed with 1x PBSBT (1X PBS, 0.5% Triton-X-100 and 1% BSA) 3x 20 min and then blocked in 1X PBSBT for 1 hour. The primary antibodies were diluted in 1X PBSBT and the brains were incubated overnight at 4C. The brains were washed in 1X PBSBT 3 x 20 min and then incubated with the respective secondary antibodies (diluted in 1X PBSBT) at 4C overnight. Next, the brains were washed with 1X PBST (1x PBS, 0.5 % Triton-X-100) 3 x 20 min and were incubated in Vectashield (Vector laboratories) mounting media at 4C. Fixed samples were imaged using a Nikon A1R HD25 laser scanning confocal microscope available at the University of Washington Biology Imaging Facility. For representative images, a 40X water objective (Nikon APO LWD, 1.15 NA) or 60X water objective (Plan Apochromat, 1.2 NA) was used and the z-step size was 0.4um.

Antibodies used for Immunohistochemistry: The following primary antibodies were used: 1:3,000 rabbit anti-Phospho-Histone H3 (Sigma H0412), 1:50 mouse anti-PKC ζ Antibody H-1

(Santa Cruz Biotechnology sc-17781), 1:1,000 mouse anti-Prospero (kind donation of the Doe lab), 1:500 guinea pig anti-Deadpan (kind donation from the Skeath lab), 1:20 rat anti-Elav (kind donation of the Doe lab), 1:1,000 rabbit anti-Numb (kind donation from the Skeath lab). Secondary antibodies were from Invitrogen and Abcam.

Live cell imaging: Media consisted of S2 Media (Sigma-Aldrich S0146) and supplemented with 10% HyClone Bovine Growth Serum (Thermo Scientific SH3054102). Third instar larvae were dissected in supplemented media and brains were transferred to a μ-slide Angiogenesis or μ-slide 8 well (Ibidi). Samples were imaged with an Intelligent Imaging Innovations (3i) spinning disc confocal system, consisting of a Yokogawa CSU-W1 spinning disc unit and two Prime 95B Scientific CMOS cameras. A 60x/1.4NA oil immersion objective mounted on a Nikon Eclipse Ti microscope was used for imaging. Live imaging voxels are 0.22 × 0.22 × 0.75-1μm (60x/1.4NA spinning disc).

Image processing and measurements: Live cell images were processed using Imaris x64 9.9.1 and Image J. Andor IQ2 files were converted into Imaris files using Imaris File Converter.

Cell size ratio: To determine the cell size ratio, at telophase the apical and basal cell diameters were measured. Using the oblique slicer, 5 1um slices were summed around the middle of the cell using Jupiter as the marker for identification. Using Myosin as a marker, a line was made from the top of the apical cortex to the middle of the cleavage furrow which provided a diameter length (um). The diameter was also calculated for basal cells, the middle of the cleavage furrow to the basal cortex. These length values were then converted to a ratio by placing the apical diameter over the basal diameter.

Deadpan and Phosphorylated Histone H3 nuclei count: Imaris's spots tool was utilized to identify Deadpan and Phosphorylated Histone H3 positive nuclei in the central brain lobe. If true positives were missed by the algorithm, these cells were identified and added manually.

Deadpan and Prospero nuclear size: To determine the nuclear size, nuclear diameter was measured. Using the oblique slicer, 12x 0.4um slices were summed around the middle of the cell using Myosin along with Deadpan or Prospero as markers for identification. Using Deadpan or Prospero as a marker a line was made through the middle of the nucleus from the top of the signal to the bottom of the signal to obtain a diameter length (um).

Lagging chromosomes: Lagging chromosomes were identified during anaphase. Any chromosome which was trailing was identified and counted according to the cortex they moved towards.

Kymographs: Average intensity projections were generated in ImageJ. All Kymographs obtained from a line drawn from the apical to the basal cortex were generated with a 10-pixel wide line.

Cell cycle timing: Cell cycle timing of resulting daughter cells were calculated from telophase to the following prophase.

Statistical analysis:

Statistical analysis was performed using Graphpad Prism 9.5. Statistical significance was determined using the appropriate method including unpaired parametric tests and nonparametric tests. Significance was indicated as the following: *; $p<0.05$, **;$p<0.01$, ***;$p<0.001$,****;$p<0.0001$, ns; not significant.

Discussion and Next Steps

ACD is a highly conserved development process which is used to create cellular diversity [53–57]. Physical asymmetry in ACD yields unequally sized sibling cells [55,58]. Although the mechanisms organisms use to establish physical ACD differ, data has begun to show that cell intrinsic mechanical forces are utilized [64]. Asymmetric spindle placement is one conserved mechanism used to establish physical ACD. For instance, sea urchin blastomeres utilize cortical pulling while mouse oocytes utilize cytoplasmic forces to establish an asymmetric spindle [7,10]. There are also spindle-independent mechanisms which can be used to establish physical ACD. For example, in *Drosophila* neuroblasts, a polarity-dependent mechanism is utilized to establish asymmetry via Myosin flows and aided by hydrostatic pressure [13–17]. In scallops, the placement of Myosin as well as Arp2/3 has been found to be critical for the establishment of physical ACD [22]. Although the general mechanisms utilized to establish physical ACD have begun to be elucidated, the molecules required to establish as well as maintain physical ACD have yet to be identified. Furthermore, one question remains of vital importance; what is the function of physical ACD?

My research has enhanced our understanding of how changes in Myosin regulation within *Drosophila* neuroblasts affects physical ACD and thereby cell fate. Using a nanobody approach, we have found alterations in Myosin localization during *Drosophila* neuroblast division can alter sibling cell fate via cell cycle timing as well as number and size of cells postulated to be neuroblasts. These findings begin to shed light on our understanding of physical ACD and supports recent discoveries in this field. Recently, a publication linking cell size and fate was released [27]. In *C. elegans*, the first embryonic division is known to be asymmetric, molecularly and physically, and gives rise to the P0. While the 3 subsequent divisions of the P lineage

resulted in cells that were asymmetric in both fate and size. However, the 4th P lineage division results in two equal sized daughter cells. Since no cell growth occurs during these 4 P lineage divisions, the authors hypothesized using mathematical models that in *C. elegans* early embryogenesis there might be a critical cell size threshold required to maintain polarity of PAR proteins and thus physical ACD. By altering the size of the first as well as second embryonic division to make a smaller P lineage, the authors found that P3 cell division resulted in equal size sibling cells and lacked PAR polarity. Thus in *C. elegans*, the P3 cell must be above the cell size threshold to establish PAR polarity which is necessary in order to undergo physical asymmetry and generate the P4 cell. This research highlights that physical cell size can guide cell fate via polarity preservation.

Moreover, new publications have begun to examine proteins involved in providing mechanical cues for proper ACD. Cazzagon et al characterized Arp2/3 branched actin filaments as well as SCAR localization during *Drosophila* neuroblast division [101]. Inhibition of Arp2/3 was found to increase the amount of apical Myosin during the onset of anaphase resulting in a slight delay of Myosin's relocalization. This finding is significant as delays in Myosin apical clearing can impact resulting sibling cell size. Additionally, Daeden et al. recently found that mislocalizing Actin, via a nanobody approach as well as an optogenetic approach, can alter physical symmetry in *Drosophila* sensory organ precursor cells [65]. Their results complement our research efforts as trapping Actin resulted in symmetric and inverted ACD. Although these authors altered cell size, any changes to cell fate which might have occurred were not assessed. Thus, how alterations to cell size may guide cell fate changes remains to be studied.

Although research has begun to elucidate some of the proteins which help establish or maintain sibling cell size, little work has been done to assess how changes in sibling cell size

cause fate changes. Jankele et al, altered spindle positioning via LIN-5 during the first *C. elegans* embryonic division in order to alter physical ACD [62]. These authors determined that there is a sibling cell size threshold required to generate viable progeny during the first division. Furthermore, changes in mitotic timing of progeny within these altered cell lineages were found to occur including positioning, division orientation as well as apoptosis. Although these authors address alterations in fate via cell cycle timing, further characterization such as examining changes in cell fate markers is absent from this study. This novel research by Jankele et al sheds light on a new focus of the field which is to understand whether a single instance of altering sibling cell size can affect subsequent progeny and result in long-term developmental consequences.

We believe this research direction is exceedingly important to gaining a deeper understanding of the function behind physical ACD. Permanently trapping Myosin in neuroblasts via a nanobody approach has contributed to our understanding of sibling cell size asymmetry. To build on our work and gain a deeper understanding, an optogenetic approach should be used to provide temporal control along with additional spatial control. Specifically, an optogenetic technique called Improved Light Induced Dimerization (iLID) would be recommended as the protein of interest can be relocalized to a domain of interest only in the presence of blue light [97]. Thus, utilizing this approach will permit direct assessment of changes in cell fate, polarity, neurogenesis as well as organismal development.

Our research has found that alterations in sibling cell size via trapping Myosin to the apical cortex of neuroblasts alters cell fate at a global level. In order to gain a clearer picture of this process, we recommend future research be conducted to alter sibling cells in a more specific manner. For instance, by trapping the Myosin in a single neuroblast or a small subset of

neuroblasts, an inverted division can be identified and alterations to cell fate as well as lineage placement can be easily recognized. We propose trapping Myosin to the apical cortex in Type 1 neuroblasts via the well characterized Gal-4 driver Ase [96]. Additionally, once further individual neuroblast Gal-4 driver lines are characterized in third instar larvae, assessing for changes to cell fate in these lineages will be enlightening.

In our studies when altering sibling cell size on a global level, we found fewer Deadpan positive cells and these cells had smaller Deadpan positive nuclei that were similar in size to wildtype Prospero positive Ganglion Mother Cell nuclei. These results suggest the small Deadpan nuclei found in nanobody expressing brains arose from inverted divisions. Based on this observation, we wonder whether these cells undergo apoptosis or differentiation. Since we did not observe small apical cells, believed to be created via inverted ACD, expressing nuclear Prospero we believe these cells do not undergo differentiation. Thus, examining cell death via a TUNEL assay for instance will provide support as to whether small Deadpan undergo apoptosis once they reach a specific cell size [102]. Moreover, we did not observe dramatic changes in neurogenesis in our studies. We suspect this may be due to the low level of inverted ACD cases which may occur as well as the potential requirement to maintain a certain cell size threshold in order to divide. However, we cannot rule out that a deeper examination may be required such as observing axonal projection patterns, distribution of synaptic connections as well as temporal identity changes. To gain a deeper understanding, we suggest altering physical asymmetry in a lineage specific manner utilizing the iLID approach. The lineage chosen should be present from larval stages into adulthood in order to assess for alterations in neurogenesis.

Overall, we speculate that there is a cell size threshold required to maintain proper cell fate within *Drosophila* neuroblasts. Sibling cells generated by symmetric division will mostly retain

their perspective fate, neuroblast and Ganglion Mother Cell, in both cell cycle timing and cell fate marker expression. These equal sized siblings can maintain proper ratio of apical to basal determinants similarly to their wildtype counterparts as they have not reached the cell size limit. However, in the case of inverted divisions, the small apical cell may express Deadpan but will not undergo subsequent division due to its physical size. We predict mechanical cues in the apical cell are relayed soon after division resulting in programmed cell death. As for the large basal cell generated during inverted divisions, the majority will retain a Ganglion Mother Cell in both cell cycle timing and Prospero expression. This retention will be due to the ratio of apical to basal determinants and not necessarily mechanical cues the cell receives. However, we postulate in a large basal cell which divides with similar timing as a wildtype neuroblast due to a combination of factors including mechanosensitive cues, amount of mRNA, organelles and proteins segregated into this cell as well as transcription and translational changes. Together these factors will guide the cell's subsequent division pattern.

Although we have begun to explore how sibling cell size affects cell fate via cell cycle timing and fate marker expression, there can also be alterations in the transcriptome. Thus, performing RNA sequencing (RNA-seq) experiments on physically altered sibling cells may enlighten us on how cells sense and respond to this change [103]. Based on our preliminary RNA-seq experiment utilizing wildtype and nanobody expressing larval brains, we identified transcripts encoding for transcription factors, G-protein coupled receptors and ion channels which exhibit different levels between these conditions (not shown here). However, we suggest further RNA-seq experiments should be conducted specifically on individual sibling cells resulting from inverted as well as symmetric divisions. Additionally, Fluorescence in situ hybridization (FISH)

may be useful technique to gain a deeper understanding of the larger transcriptome changes [104].

Moreover, our research has shown that inverting molecular asymmetry affects cell fate via cell cycle timing as well as the number and nuclear size of cells postulated to have a neuroblast fate. Specifically, trapping the scaffolding protein Miranda results in altered localization of the basal cell fate determinant Prospero. This research is novel as to our knowledge, inverted molecular asymmetry by the mislocalization of a scaffolding protein, thus altering basal fate determinants, has not been reported in flies, humans, mice or worms. The most relevant research was conducted to misalign the miotic spindle in order to make it orthogonal to apical/basal polarity in *Drosophila* neuroblasts thus altering cell determinants localization [79]. They found that basal determinants can be segregated into one sibling, while expressing neuroblast fate markers, and not induce differentiation to a Ganglion Mother Cell like fate. Thus, the ratio of apical to basal determinants affects neuroblast and Ganglion Mother Cell fate via cell cycle timing as well as cell fate markers. We believe future research should be conducted to trap individual as well as multiple basal fate determinants in neuroblasts and assess for fate changes. Findings from these experiments will allow us to gain a deeper understanding of the requirements behind ACD maintenance.

Although our current model highlights Pkn's instrumental role in symmetry breaking, we have yet to: 1) Determine whether mislocalization of Pkn is sufficient to alter symmetry breaking. 2) Determine the crucial time in which Pkn must be present on the apical cortex to break symmetry. Future research should be conducted to trap Pkn separately to the apical or basal cortex of neuroblasts and assessed for alterations in Myosin's spatiotemporal dynamics. Furthermore, the iLID approach should be utilized to relocalize Pkn to the apical cortex of

neuroblasts during certain stages during mitosis, particularly prophase and metaphase, and examined for changes in Myosin dynamics. If these results show symmetry breakage can arise earlier in mitosis just by the misplacement of Pkn, we suspect alterations in sibling cell size will be observed.

Utilizing the *pkn* mutant fly line predicted to contain a truncated Pkn kinase domain, we found that the spatiotemporal dynamics of Myosin in *Drosophila* neuroblasts is altered. These results confirm the previously published *pkn* mutant phenotype. Future research should be conducted to determine whether Pkn's kinase domain is critical for Myosin's proper spatiotemporal dynamics. We recommend generating a fly line in which the kinase domain be removed via CRISPR. Once the line is made, it should be examined for changes in Myosin's dynamics within neuroblasts. If changes are observed, single amino acid substitutions should be to the Pkn kinase domain in order to determine what amino acids are important.

Although Pkn's novel role in *Drosophila* neuroblast symmetry breaking was published by Tsankova et al in 2017, no additional publications have been released focused on Pkn's role in ACD or other mechano-related functions in flies nor other organisms such as humans, mice or worms [17]. This highlights the critical need for more research regarding this protein and its binding partners. Our research has identified numerous potential binding partners of Pkn via pull-down assays. We suggest future research utilize our list of potential binding partners of Pkn identified to assess whether these proteins, via RNAi and mutants fly lines, alter Myosin's spatiotemporal dynamics.

One candidate which requires further examination is Sgg. Although we did not observe a phenotype while characterizing a single mutant line listed as a hypomorphic and amorphic allele, we believe characterization of other amorphic alleles will show altered Myosin dynamics similar

to those found in *pkn* mutants. After initial characterization is complete of all potential binding partners, those proteins which show promise should be further analyzed to determine whether they directly interact with Pkn. Three candidates for possible physical interaction include Sgg, Pins and Lgl. Currently no information is available which supports which, if any, region of Sgg or Pins bind directly to Pkn. Thus, we suggest a preliminary assessment be conducted to compile a list of potential domains of interest. Once obtained, Sgg or Pins lines should be generated or if possible, utilize existing *sgg* or *pins* mutant lines. After the lines are generated, live cell imaging should be conducted to determine whether Myosin's as well as Pkn's dynamics are altered. Once the potential domains have been narrowed down, reciprocal pull-downs should be conducted to determine whether Pkn directly interacts with Sgg as well as Pins at these domains.

In *Drosophila*, Lgl is known to be phosphorylated by aPKC at 3 different Serine residues (656, 660, 664) resulting in Lgl to undergo confirmational changes in which it can no longer interact with Myosin's heavy chain resulting in Lgl's basal segregation thus ensuring apical polarity establishment [92–94]. We wonder if Pkn may directly phosphorylate Lgl alongside aPKC to remove any residual Lgl interacting with Myosin's heavy chain and thus disrupt Myosin's localization on the apical cortex resulting in asymmetry breaking. To provide support for this, we noted *Drosophila* Pkn protein sequence is highly conserved with human Pkn 1, Pkn 2 and human Pkn 3. Since Pkn's kinase domains consensus motif is not known in *Drosophila*, we wondered whether the consensus motif of human Pkn 1 and Pkn 3 could recognize any sites on *Drosophila* Lgl [95]. We found that S656 on *Drosophila* Lgl is recognized by human Pkn 1 and Pkn 3 which may also be utilized by *Drosophila* Pkn. Thus, we suggest future research should be conducted to determine whether *Drosophila* neuroblasts Pkn directly interacts with Lgl at this site. A fly line containing a single amino acid substitution at S656 in Lgl via CRISPR to remove

the potential consensus sequence should be generated. Once generated, reciprocal pull-downs with Pkn and mutated Lgl, alongside controls, ought to be conducted to assess whether Lgl and Pkn directly interact at this site. Additionally, live cell imaging should be conducted on this Lgl fly line to confirm whether Myosin dynamics are altered when this consensus region of Lgl is no longer present. We speculate that Pkn may directly phosphorylate Lgl as well as Sgg in metaphase to allow for Myosin's movement from the apical cortex. Together these proteins will work with previously reported polarity proteins to establish symmetry breaking event required for proper physical ACD in *Drosophila* neuroblasts.

Our research begins to elucidate the molecular mechanisms as well as functions behind physical asymmetry. Determining the proteins upstream and downstream of Pkn required for proper Myosin's dynamics will be instrumental in gaining a deeper understanding of physical ACD. Since many cell types and organisms undergo physical ACD, our results are an important steppingstone for further studies. It is our hope that our research spurs interest in elucidating the mechanisms and functions of physical ACD.

BIBLIOGRAPHY

1. Horvitz, H.R.; Herskowitz, I. Mechanisms of Asymmetric Cell Division: Two Bs or Not Two Bs, That Is the Question. *Cell* **1992**, *68*, 237–255, doi:10.1016/0092-8674(92)90468-r.

2. Poon, J.; Fries, A.; Wessel, G.M.; Yajima, M. Evolutionary Modification of AGS Protein Contributes to Formation of Micromeres in Sea Urchins. *Nat Commun* **2019**, *10*, 3779, doi:10.1038/s41467-019-11560-8.

3. Kiyomitsu, T. The Cortical Force-Generating Machinery: How Cortical Spindle-Pulling Forces Are Generated. *Curr Opin Cell Biol* **2019**, *60*, 1–8, doi:10.1016/j.ceb.2019.03.001.

4. Sallé, J.; Xie, J.; Ershov, D.; Lacassin, M.; Dmitrieff, S.; Minc, N. Asymmetric Division through a Reduction of Microtubule Centering ForcesCentering Forces Control Asymmetric Division. *J Cell Biology* **2019**, *218*, 771–782, doi:10.1083/jcb.201807102.

5. Kotak, S. Mechanisms of Spindle Positioning: Lessons from Worms and Mammalian Cells. *Biomol* **2019**, *9*, 80, doi:10.3390/biom9020080.

6. Mogessie, B.; Scheffler, K.; Schuh, M. Assembly and Positioning of the Oocyte Meiotic Spindle. *Annu Rev Cell Dev Bi* **2018**, *34*, 381–403, doi:10.1146/annurev-cellbio-100616-060553.

7. Duan, X.; Li, Y.; Yi, K.; Guo, F.; Wang, H.; Wu, P.-H.; Yang, J.; Mair, D.B.; Morales, E.A.; Kalab, P.; et al. Dynamic Organelle Distribution Initiates Actin-Based Spindle Migration in Mouse Oocytes. *Nat Commun* **2020**, *11*, 277, doi:10.1038/s41467-019-14068-3.

8. Wei, Z.; Greaney, J.; Zhou, C.; Homer, H.A. Cdk1 Inactivation Induces Post-Anaphase-Onset Spindle Migration and Membrane Protrusion Required for Extreme Asymmetry in Mouse Oocytes. *Nat Commun* **2018**, *9*, 4029, doi:10.1038/s41467-018-06510-9.

9. Yi, K.; Unruh, J.R.; Deng, M.; Slaughter, B.D.; Rubinstein, B.; Li, R. Dynamic Maintenance of Asymmetric Meiotic Spindle Position through Arp2/3-Complex-Driven Cytoplasmic Streaming in Mouse Oocytes. *Nat Cell Biol* **2011**, *13*, 1252–1258, doi:10.1038/ncb2320.

10. Wang, H.; Li, Y.; Yang, J.; Duan, X.; Kalab, P.; Sun, S.X.; Li, R. Symmetry Breaking in Hydrodynamic Forces Drives Meiotic Spindle Rotation in Mammalian Oocytes. *Sci Adv* **2020**, *6*, eaaz5004, doi:10.1126/sciadv.aaz5004.

11. Basant, A.; Glotzer, M. Spatiotemporal Regulation of RhoA during Cytokinesis. *Curr Biol* **2018**, *28*, R570–R580, doi:10.1016/j.cub.2018.03.045.

12. Gallaud, E.; Pham, T.; Cabernard, C. Asymmetric Cell Division in Development, Differentiation and Cancer. *Results Problems Cell Differ* **2017**, *61*, 183–210, doi:10.1007/978-3-319-53150-2_8.

13. Cabernard, C.; Prehoda, K.E.; Doe, C.Q. A Spindle-Independent Cleavage Furrow Positioning Pathway. *Nature* **2010**, *467*, 91–94, doi:10.1038/nature09334.

14. Connell, M.; Cabernard, C.; Ricketson, D.; Doe, C.Q.; Prehoda, K.E. Asymmetric Cortical Extension Shifts Cleavage Furrow Position in Drosophila Neuroblasts. *Mol Biol Cell* **2011**, *22*, 4220–4226, doi:10.1091/mbc.e11-02-0173.

15. Roth, M.; Roubinet, C.; Iffländer, N.; Ferrand, A.; Cabernard, C. Asymmetrically Dividing Drosophila Neuroblasts Utilize Two Spatially and Temporally Independent Cytokinesis Pathways. *Nat Commun* **2015**, *6*, 6551, doi:10.1038/ncomms7551.

16. Roubinet, C.; Tsankova, A.; Pham, T.T.; Monnard, A.; Caussinus, E.; Affolter, M.; Cabernard, C. Spatio-Temporally Separated Cortical Flows and Spindle Geometry Establish Physical Asymmetry in Fly Neural Stem Cells. *Nat Commun* **2017**, *8*, 1383, doi:10.1038/s41467-017-01391-w.

17. Tsankova, A.; Pham, T.T.; Garcia, D.S.; Otte, F.; Cabernard, C. Cell Polarity Regulates Biased Myosin Activity and Dynamics during Asymmetric Cell Division via Drosophila Rho Kinase and Protein Kinase N. *Dev Cell* **2017**, *42*, 143-155.e5, doi:10.1016/j.devcel.2017.06.012.

18. Pham, T.T.; Monnard, A.; Helenius, J.; Lund, E.; Lee, N.; Müller, D.J.; Cabernard, C. Spatiotemporally Controlled Myosin Relocalization and Internal Pressure Cause Biased Cortical Extension to Generate Sibling Cell Size Asymmetry. *Iscience* **2019**, *13*, 9–19, doi:10.1016/j.isci.2019.02.002.

19. Klinkert, K.; Levernier, N.; Gross, P.; Gentili, C.; Tobel, L. von; Pierron, M.; Busso, C.; Herrman, S.; Grill, S.W.; Kruse, K.; et al. Aurora A Depletion Reveals Centrosome-Independent Polarization Mechanism in Caenorhabditis Elegans. *Elife* **2019**, *8*, e44552, doi:10.7554/elife.44552.

20. Zhao, P.; Teng, X.; Tantirimudalige, S.N.; Nishikawa, M.; Wohland, T.; Toyama, Y.; Motegi, F. Aurora-A Breaks Symmetry in Contractile Actomyosin Networks Independently of Its Role in Centrosome Maturation. *Dev Cell* **2019**, *48*, 631-645.e6, doi:10.1016/j.devcel.2019.02.012.

21. Goulding, M.Q.; Lambert, J.D. Mollusc Models I. The Snail Ilyanassa. *Curr Opin Genet Dev* **2016**, *39*, 168–174, doi:10.1016/j.gde.2016.07.007.

22. Toledo-Jacobo, L.; Henson, J.H.; Shuster, C.B. Cytoskeletal Polarization and Cytokinetic Signaling Drives Polar Lobe Formation in Spiralian Embryos. *Dev Biol* **2019**, doi:10.1016/j.ydbio.2019.08.020.

23. Atkinson, J.W. Organogenesis in Normal and Lobeless Embryos of the Marine Prosobranch Gastropod Ilyanassa Obsoleta. *J. Morphol.* **1971**, *133*, 339–352, doi:10.1002/jmor.1051330307.

24. Clement, A.C. Experimental Studies on Germinal Localization in Ilyanassa. I. The Role of the Polar Lobe in Determination of the Cleavage Pattern and Its Influence in Later Development. *J. Exp. Zool.* **1952**, *121*, 593–625, doi:10.1002/jez.1401210310.

25. Crampton, H.E.; Wilson, E.B. Experimental Studies on Gasteropod Development. *Archiv Für Entwicklungsmechanik Der Org* **1896**, *3*, 1–19, doi:10.1007/bf02156309.

26. Render, J. Development of Ilyanassa Obsoleta Embryos after Equal Distribution of Polar Lobe Material at First Cleavage. *Dev Biol* **1989**, *132*, 241–250, doi:10.1016/0012-1606(89)90220-0.

27. Hubatsch, L.; Peglion, F.; Reich, J.D.; Rodrigues, N.T.L.; Hirani, N.; Illukkumbura, R.; Goehring, N.W. A Cell-Size Threshold Limits Cell Polarity and Asymmetric Division Potential. *Nat Phys* **2019**, 1–8, doi:10.1038/s41567-019-0601-x.

28. Dasgupta, I.; McCollum, D. Control of Cellular Responses to Mechanical Cues through YAP/TAZ Regulation. *J Biological Chem* **2019**, *294*, 17693–17706, doi:10.1074/jbc.rev119.007963.

29. Nishioka, N.; Inoue, K.; Adachi, K.; Kiyonari, H.; Ota, M.; Ralston, A.; Yabuta, N.; Hirahara, S.; Stephenson, R.O.; Ogonuki, N.; et al. The Hippo Signaling Pathway Components Lats and Yap Pattern Tead4 Activity to Distinguish Mouse Trophectoderm from Inner Cell Mass. *Dev Cell* **2009**, *16*, 398–410, doi:10.1016/j.devcel.2009.02.003.

30. Kang, P.H.; Schaffer, D.V.; Kumar, S. Angiomotin Links ROCK and YAP Signaling in Mechanosensitive Differentiation of Neural Stem Cells. *Mol Biol Cell* **2020**, mbcE19110602, doi:10.1091/mbc.e19-11-0602.

31. Zaltsman, Y.; Masuko, S.; Bensen, J.J.; Kiessling, L.L. Angiomotin Regulates YAP Localization during Neural Differentiation of Human Pluripotent Stem Cells. *Stem Cell Rep* **2019**, *12*, 869–877, doi:10.1016/j.stemcr.2019.03.009.

32. Hirate, Y.; Hirahara, S.; Inoue, K.; Suzuki, A.; Alarcon, V.B.; Akimoto, K.; Hirai, T.; Hara, T.; Adachi, M.; Chida, K.; et al. Polarity-Dependent Distribution of Angiomotin Localizes Hippo Signaling in Preimplantation Embryos. *Curr Biol* **2013**, *23*, 1181–1194, doi:10.1016/j.cub.2013.05.014.

33. Samarage, C.R.; White, M.D.; Álvarez, Y.D.; Fierro-González, J.C.; Henon, Y.; Jesudason, E.C.; Bissiere, S.; Fouras, A.; Plachta, N. Cortical Tension Allocates the First Inner Cells of the Mammalian Embryo. *Dev Cell* **2015**, *34*, 435–447, doi:10.1016/j.devcel.2015.07.004.

34. Maître, J.-L.; Turlier, H.; Illukkumbura, R.; Eismann, B.; Niwayama, R.; Nédélec, F.; Hiiragi, T. Asymmetric Division of Contractile Domains Couples Cell Positioning and Fate Specification. *Nature* **2016**, *536*, 344, doi:10.1038/nature18958.

35. Gonzalez, N.P.; Tao, J.; Rochman, N.D.; Vig, D.; Chiu, E.; Wirtz, D.; Sun, S.X. Cell Tension and Mechanical Regulation of Cell Volume. *Mol Biol Cell* **2018**, *29*, 0–0, doi:10.1091/mbc.e18-04-0213.

36. Elosegui-Artola, A.; Andreu, I.; Beedle, A.E.M.; Lezamiz, A.; Uroz, M.; Kosmalska, A.J.; Oria, R.; Kechagia, J.Z.; Rico-Lastres, P.; Roux, A.-L.L.; et al. Force Triggers YAP Nuclear Entry by Regulating Transport across Nuclear Pores. *Cell* **2017**, *171*, 1397-1410.e14, doi:10.1016/j.cell.2017.10.008.

37. Sugimoto, A.; Miyazaki, A.; Kawarabayashi, K.; Shono, M.; Akazawa, Y.; Hasegawa, T.; Ueda-Yamaguchi, K.; Kitamura, T.; Yoshizaki, K.; Fukumoto, S.; et al. Piezo Type Mechanosensitive Ion Channel Component 1 Functions as a Regulator of the Cell Fate Determination of Mesenchymal Stem Cells. *Sci Rep-uk* **2017**, *7*, 17696, doi:10.1038/s41598-017-18089-0.

38. Gudipaty, S.A.; Lindblom, J.; Loftus, P.D.; Redd, M.J.; Edes, K.; Davey, C.F.; Krishnegowda, V.; Rosenblatt, J. Mechanical Stretch Triggers Rapid Epithelial Cell Division through Piezo1. *Nature* **2017**, *543*, 118–121, doi:10.1038/nature21407.

39. Pathak, M.M.; Nourse, J.L.; Tran, T.; Hwe, J.; Arulmoli, J.; Le, D.T.T.; Bernardis, E.; Flanagan, L.A.; Tombola, F. Stretch-Activated Ion Channel Piezo1 Directs Lineage Choice in Human Neural Stem Cells. *P Natl Acad Sci Usa* **2014**, *111*, 16148–16153, doi:10.1073/pnas.1409802111.

40. He, L.; Si, G.; Huang, J.; Samuel, A.D.T.; Perrimon, N. Mechanical Regulation of Stem-Cell Differentiation by the Stretch-Activated Piezo Channel. *Nature* **2018**, *555*, 103 106, doi:10.1038/nature25744.

41. Micchelli, C.A.; Perrimon, N. Evidence That Stem Cells Reside in the Adult Drosophila Midgut Epithelium. *Nature* **2006**, *439*, 475–479, doi:10.1038/nature04371.

42. Ohlstein, B.; Spradling, A. The Adult Drosophila Posterior Midgut Is Maintained by Pluripotent Stem Cells. *Nature* **2006**, *439*, 470–474, doi:10.1038/nature04333.

43. Goulas, S.; Conder, R.; Knoblich, J.A. The Par Complex and Integrins Direct Asymmetric Cell Division in Adult Intestinal Stem Cells. *Cell Stem Cell* **2012**, *11*, 529–540, doi:10.1016/j.stem.2012.06.017.

44. Ellefsen, K.L.; Holt, J.R.; Chang, A.C.; Nourse, J.L.; Arulmoli, J.; Mekhdjian, A.H.; Abuwarda, H.; Tombola, F.; Flanagan, L.A.; Dunn, A.R.; et al. Myosin-II Mediated Traction Forces Evoke Localized Piezo1-Dependent Ca2+ Flickers. *Commun Biology* **2019**, *2*, 298, doi:10.1038/s42003-019-0514-3.

45. Sugioka, K.; Bowerman, B. Combinatorial Contact Cues Specify Cell Division Orientation by Directing Cortical Myosin Flows. *Dev Cell* **2018**, *46*, 257-270.e5, doi:10.1016/j.devcel.2018.06.020.

46. Korotkevich, E.; Niwayama, R.; Courtois, A.; Friese, S.; Berger, N.; Buchholz, F.; Hiiragi, T. The Apical Domain Is Required and Sufficient for the First Lineage Segregation in the Mouse Embryo. *Dev Cell* **2017**, *40*, 235-247.e7, doi:10.1016/j.devcel.2017.01.006.

47. Anani, S.; Bhat, S.; Honma-Yamanaka, N.; Krawchuk, D.; Yamanaka, Y. Initiation of Hippo Signaling Is Linked to Polarity Rather than to Cell Position in the Pre-Implantation Mouse Embryo. *Development* **2014**, *141*, 2813–2824, doi:10.1242/dev.107276.

48. Watanabe, T.; Biggins, J.S.; Tannan, N.B.; Srinivas, S. Limited Predictive Value of Blastomere Angle of Division in Trophectoderm and Inner Cell Mass Specification. *Development* **2014**, *141*, 2279–2288, doi:10.1242/dev.103267.

49. Leen, E.V. van; Pietro, F. di; Bellaïche, Y. Oriented Cell Divisions in Epithelia: From Force Generation to Force Anisotropy by Tension, Shape and Vertices. *Curr Opin Cell Biol* **2020**, *62*, 9–16, doi:10.1016/j.ceb.2019.07.013.

50. Niwayama, R.; Moghe, P.; Liu, Y.-J.; Fabrèges, D.; Buchholz, F.; Piel, M.; Hiiragi, T. A Tug-of-War between Cell Shape and Polarity Controls Division Orientation to Ensure Robust Patterning in the Mouse Blastocyst. *Dev Cell* **2019**, *51*, 564-574.e6, doi:10.1016/j.devcel.2019.10.012.

51. Loyer, N.; Januschke, J. The Last-Born Daughter Cell Contributes to Division Orientation of Drosophila Larval Neuroblasts. *Nat Commun* **2018**, *9*, 3745, doi:10.1038/s41467-018-06276-0.

52. Chan, C.J.; Costanzo, M.; Ruiz-Herrero, T.; Mönke, G.; Petrie, R.J.; Bergert, M.; Diz-Muñoz, A.; Mahadevan, L.; Hiiragi, T. Hydraulic Control of Mammalian Embryo Size and Cell Fate. *Nature* **2019**, *571*, 112–116, doi:10.1038/s41586-019-1309-x.

53. Harding, K.; White, K. Drosophila as a Model for Developmental Biology: Stem Cell-Fate Decisions in the Developing Nervous System. *J Dev Biology* **2018**, *6*, 25, doi:10.3390/jdb6040025.

54. Santoro, A.; Vlachou, T.; Carminati, M.; Pelicci, P.G.; Mapelli, M. Molecular Mechanisms of Asymmetric Divisions in Mammary Stem Cells. *Embo Rep* **2016**, *17*, 1700–1720, doi:10.15252/embr.201643021.

55. Sunchu, B.; Cabernard, C. Principles and Mechanisms of Asymmetric Cell Division. *Development* **2020**, *147*, dev167650, doi:10.1242/dev.167650.

56. Venkei, Z.G.; Yamashita, Y.M. Emerging Mechanisms of Asymmetric Stem Cell Division. *J Cell Biol* **2018**, *217*, jcb.201807037, doi:10.1083/jcb.201807037.

57. Vertii, A.; Kaufman, P.D.; Hehnly, H.; Doxsey, S. New Dimensions of Asymmetric Division in Vertebrates. *Cytoskeleton* **2018**, *75*, 87–102, doi:10.1002/cm.21434.

58. Homem, C.C.F.; Knoblich, J.A. Drosophila Neuroblasts: A Model for Stem Cell Biology. *Development* **2012**, *139*, 4297–4310, doi:10.1242/dev.080515.

59. Knoblich, J.A. Asymmetric Cell Division: Recent Developments and Their Implications for Tumour Biology. *Nat Rev Mol Cell Bio* **2010**, *11*, 849–860, doi:10.1038/nrm3010.

60. Li, Z.; Zhang, Y.Y.; Zhang, H.; Yang, J.; Chen, Y.; Lu, H. Asymmetric Cell Division and Tumor Heterogeneity. *Frontiers Cell Dev Biology* **2022**, *10*, 938685, doi:10.3389/fcell.2022.938685.

61. *Asymmetric Cell Division in Development, Differentiation and Cancer*; Tassan, J.-P., Kubiak, J.Z., Eds.; 2017; Vol. 61; ISBN 978-3-319-53149-6.

62. Jankele, R.; Jelier, R.; Gönczy, P. Physically Asymmetric Division of the C. Elegans Zygote Ensures Invariably Successful Embryogenesis. *Elife* **2021**, *10*, e61714, doi:10.7554/elife.61714.

63. Hitomi, M.; Chumakova, A.P.; Silver, D.J.; Knudsen, A.M.; Pontius, W.D.; Murphy, S.; Anand, N.S.; Kristensen, B.W.; Lathia, J. Asymmetric Cell Division Promotes Therapeutic Resistance in Glioblastoma Stem Cells. *Jci Insight* **2020**, *6*, e130510, doi:10.1172/jci.insight.130510.

64. Delgado, M.K.; Cabernard, C. Mechanical Regulation of Cell Size, Fate, and Behavior during Asymmetric Cell Division. *Curr Opin Cell Biol* **2020**, *67*, 9–16, doi:10.1016/j.ceb.2020.07.002.

65. Daeden, A.; Mietke, A.; Derivery, E.; Seum, C.; Jülicher, F.; Gonzalez-Gaitan, M. Polarized Branched Actin Modulates Cortical Mechanics to Produce Unequal-Size Daughters during Asymmetric Division. *Nat Cell Biol* **2023**, 1–11, doi:10.1038/s41556-022-01058-9.

66. Lim, Y.W.; Wen, F.-L.; Shankar, P.; Shibata, T.; Motegi, F. A Balance between Antagonizing PAR Proteins Specifies the Pattern of Asymmetric and Symmetric Divisions in C. Elegans Embryogenesis. *Cell Reports* **2021**, *36*, 109326, doi:10.1016/j.celrep.2021.109326.

67. Chai, Y.; Tian, D.; Zhu, Z.; Jiang, Y.; Huang, S.; Wu, D.; Ou, G.; Li, W. Wnt Signaling Polarizes Cortical Actin Polymerization to Increase Daughter Cell Asymmetry. *Cell Discov* **2022**, *8*, 22, doi:10.1038/s41421-022-00376-4.

68. Ou, G.; Stuurman, N.; D'Ambrosio, M.; Vale, R.D. Polarized Myosin Produces Unequal-Size Daughters During Asymmetric Cell Division. *Science* **2010**, *330*, 677–680, doi:10.1126/science.1196112.

69. Ferreira, T.; Prudêncio, P.; Martinho, R.G. Drosophila Protein Kinase N (Pkn) Is a Negative Regulator of Actin–Myosin Activity during Oogenesis. *Dev Biol* **2014**, *394*, 277–291, doi:10.1016/j.ydbio.2014.08.008.

70. Bagci, H.; Sriskandarajah, N.; Robert, A.; Boulais, J.; Elkholi, I.E.; Tran, V.; Lin, Z.-Y.; Thibault, M.-P.; Dubé, N.; Faubert, D.; et al. Mapping the Proximity Interaction Network of the Rho-Family GTPases Reveals Signalling Pathways and Regulatory Mechanisms. *Nat Cell Biol* **2020**, *22*, 120–134, doi:10.1038/s41556-019-0438-7.

71. Betson, M.; Settleman, J. A Rho-Binding Protein Kinase C-Like Activity Is Required for the Function of Protein Kinase N in Drosophila Development. *Genetics* **2007**, *176*, 2201–2212, doi:10.1534/genetics.107.072967.

72. Friedman, A.A.; Tucker, G.; Singh, R.; Yan, D.; Vinayagam, A.; Hu, Y.; Binari, R.; Hong, P.; Sun, X.; Porto, M.; et al. Proteomic and Functional Genomic Landscape of Receptor Tyrosine Kinase and Ras to Extracellular Signal–Regulated Kinase Signaling. *Sci Signal* **2011**, *4*, rs10, doi:10.1126/scisignal.2002029.

73. Emani, M.R.; Närvä, E.; Stubb, A.; Chakroborty, D.; Viitala, M.; Rokka, A.; Rahkonen, N.; Moulder, R.; Denessiouk, K.; Trokovic, R.; et al. The L1TD1 Protein Interactome Reveals the Importance of Post-Transcriptional Regulation in Human Pluripotency. *Stem Cell Rep* **2015**, *4*, 519–528, doi:10.1016/j.stemcr.2015.01.014.

74. Lee, J.H.; Han, J.; Kim, H.; Park, S.M.; Joe, E.; Jou, I. Parkinson's Disease-Associated LRRK2-G2019S Mutant Acts through Regulation of SERCA Activity to Control ER Stress in Astrocytes. *Acta Neuropathologica Commun* **2019**, *7*, 68, doi:10.1186/s40478-019-0716-4.

75. Riffle, M.; Hoopmann, M.R.; Jaschob, D.; Zhong, G.; Moritz, R.L.; MacCoss, M.J.; Davis, T.N.; Isoherranen, N.; Zelter, A. Discovery and Visualization of Uncharacterized Drug–Protein Adducts Using Mass Spectrometry. *Anal Chem* **2022**, *94*, 3501–3509, doi:10.1021/acs.analchem.1c04101.

76. Betschinger, J.; Eisenhaber, F.; Knoblich, J.A. Phosphorylation-Induced Autoinhibition Regulates the Cytoskeletal Protein Lethal (2) Giant Larvae. *Curr Biol* **2005**, *15*, 276–282, doi:10.1016/j.cub.2005.01.012.

77. Albertson, R.; Doe, C.Q. Dlg, Scrib and Lgl Regulate Neuroblast Cell Size and Mitotic Spindle Asymmetry. *Nat Cell Biol* **2003**, *5*, 166–170, doi:10.1038/ncb922.

78. Caussinus, E.; Kanca, O.; Affolter, M. Fluorescent Fusion Protein Knockout Mediated by Anti-GFP Nanobody. *Nat Struct Mol Biol* **2012**, *19*, 117, doi:10.1038/nsmb.2180.

79. Cabernard, C.; Doe, C.Q. Apical/Basal Spindle Orientation Is Required for Neuroblast Homeostasis and Neuronal Differentiation in Drosophila. *Dev Cell* **2009**, *17*, 134–141, doi:10.1016/j.devcel.2009.06.009.

80. Homem, C.C.F.; Reichardt, I.; Berger, C.; Lendl, T.; Knoblich, J.A. Long-Term Live Cell Imaging and Automated 4D Analysis of Drosophila Neuroblast Lineages. *Plos One* **2013**, *8*, e79588, doi:10.1371/journal.pone.0079588.

81. Choksi, S.P.; Southall, T.D.; Bossing, T.; Edoff, K.; Wit, E. de; Fischer, B.E.; Steensel, B. van; Micklem, G.; Brand, A.H. Prospero Acts as a Binary Switch between Self-Renewal and Differentiation in Drosophila Neural Stem Cells. *Dev Cell* **2006**, *11*, 775–789, doi:10.1016/j.devcel.2006.09.015.

82. Doe, C.Q.; Chu-LaGraff, Q.; Wright, D.M.; Scott, M.P. The Prospero Gene Specifies Cell Fates in the Drosophila Central Nervous System. *Cell* **1991**, *65*, 451–464, doi:10.1016/0092-8674(91)90463-9.

83. San-Juán, B.P.; Baonza, A. The BHLH Factor Deadpan Is a Direct Target of Notch Signaling and Regulates Neuroblast Self-Renewal in Drosophila. *Dev Biol* **2011**, *352*, 70–82, doi:10.1016/j.ydbio.2011.01.019.

84. Berger, C.; Renner, S.; Lüer, K.; Technau, G.M. The Commonly Used Marker ELAV Is Transiently Expressed in Neuroblasts and Glial Cells in the Drosophila Embryonic CNS. *Dev. Dyn.* **2007**, *236*, 3562–3568, doi:10.1002/dvdy.21372.

85. Deng, Q.; Wang, H. Re-Visiting the Principles of Apicobasal Polarity in Drosophila Neural Stem Cells. *Dev Biol* **2022**, *484*, 57–62, doi:10.1016/j.ydbio.2022.02.006.

86. Ikeshima-Kataoka, H.; Skeath, J.B.; Nabeshima, Y.; Doe, C.Q.; Matsuzaki, F. Miranda Directs Prospero to a Daughter Cell during Drosophila Asymmetric Divisions. *Nature* **1997**, *390*, 625–629, doi:10.1038/37641.

87. Lee, C.-Y.; Wilkinson, B.D.; Siegrist, S.E.; Wharton, R.P.; Doe, C.Q. Brat Is a Miranda Cargo Protein That Promotes Neuronal Differentiation and Inhibits Neuroblast Self-Renewal. *Dev Cell* **2006**, *10*, 441–449, doi:10.1016/j.devcel.2006.01.017.

88. Shen, C.-P.; Knoblich, J.A.; Chan, Y.-M.; Jiang, M.-M.; Jan, L.Y.; Jan, Y.N. Miranda as a Multidomain Adapter Linking Apically Localized Inscuteable and Basally Localized Staufen and Prospero during Asymmetric Cell Division InDrosophila. *Gene Dev* **1998**, *12*, 1837–1846, doi:10.1101/gad.12.12.1837.

89. Shen, C.-P.; Jan, L.Y.; Jan, Y.N. Miranda Is Required for the Asymmetric Localization of Prospero during Mitosis in Drosophila. *Cell* **1997**, *90*, 449–458, doi:10.1016/s0092-8674(00)80505-x.

90. Bhalerao, S.; Berdnik, D.; Török, T.; Knoblich, J.A. Localization-Dependent and -Independent Roles of Numb Contribute to Cell-Fate Specification in Drosophila. *Curr Biol* **2005**, *15*, 1583–1590, doi:10.1016/j.cub.2005.07.061.

91. Lu, B.; Rothenberg, M.; Jan, L.Y.; Jan, Y.N. Partner of Numb Colocalizes with Numb during Mitosis and Directs Numb Asymmetric Localization in Drosophila Neural and Muscle Progenitors. *Cell* **1998**, *95*, 225–235, doi:10.1016/s0092-8674(00)81753-5.

92. Bell, G.P.; Fletcher, G.C.; Brain, R.; Thompson, B.J. Aurora Kinases Phosphorylate Lgl to Induce Mitotic Spindle Orientation in Drosophila Epithelia. *Curr Biol* **2015**, *25*, 61–68, doi:10.1016/j.cub.2014.10.052.

93. Moreira, S.; Morais-de-Sá, E. Spatiotemporal Phosphoregulation of Lgl: Finding Meaning in Multiple on/off Buttons. *Bioarchitecture* **2016**, *6*, 29–38, doi:10.1080/19490992.2016.1149290.

94. Zhu, J.; Shang, Y.; Wan, Q.; Xia, Y.; Chen, J.; Du, Q.; Zhang, M. Phosphorylation-Dependent Interaction between Tumor Suppressors Dlg and Lgl. *Cell Res* **2014**, *24*, 451–463, doi:10.1038/cr.2014.16.

95. Collazos, A.; Michael, N.; Whelan, R.D.H.; Kelly, G.; Mellor, H.; Pang, L.C.H.; Totty, N.; Parker, P.J. Site Recognition and Substrate Screens for PKN Family Proteins. *Biochem J* **2011**, *438*, 535–543, doi:10.1042/bj20110521.

96. Jiang, Y.; Reichert, H. Drosophila Neural Stem Cells in Brain Development and Tumor Formation. *J Neurogenet* **2014**, *28*, 181–189, doi:10.3109/01677063.2014.898639.

97. Guntas, G.; Hallett, R.A.; Zimmerman, S.P.; Williams, T.; Yumerefendi, H.; Bear, J.E.; Kuhlman, B. Engineering an Improved Light-Induced Dimer (ILID) for Controlling the Localization and Activity of Signaling Proteins. *Proc National Acad Sci* **2015**, *112*, 112–117, doi:10.1073/pnas.1417910112.

98. Chambers, M.C.; Maclean, B.; Burke, R.; Amodei, D.; Ruderman, D.L.; Neumann, S.; Gatto, L.; Fischer, B.; Pratt, B.; Egertson, J.; et al. A Cross-Platform Toolkit for Mass Spectrometry and Proteomics. *Nat Biotechnol* **2012**, *30*, 918–920, doi:10.1038/nbt.2377.

99. Eng, J.K.; Jahan, T.A.; Hoopmann, M.R. Comet: An Open-source MS/MS Sequence Database Search Tool. *Proteomics* **2013**, *13*, 22–24, doi:10.1002/pmic.201200439.

100. Käll, L.; Canterbury, J.D.; Weston, J.; Noble, W.S.; MacCoss, M.J. Semi-Supervised Learning for Peptide Identification from Shotgun Proteomics Datasets. *Nat Methods* **2007**, *4*, 923–925, doi:10.1038/nmeth1113.

101. Cazzagon, G.; Roubinet, C.; Baum, B. SCAR and the Arp2/3 Complex Polarise the Actomyosin Cortex and Plasma Membrane Organization in Asymmetrically Dividing Neuroblasts. **2023**, doi:10.1101/2023.01.05.522888.

102. Denton, D.; Mills, K.; Kumar, S. Chapter 2 Methods and Protocols for Studying Cell Death in Drosophila. *Methods Enzymol* **2008**, *446*, 17–37, doi:10.1016/s0076-6879(08)01602-9.

103. Stark, R.; Grzelak, M.; Hadfield, J. RNA Sequencing: The Teenage Years. *Nat Rev Genet* **2019**, *20*, 631–656, doi:10.1038/s41576-019-0150-2.

104. Nath, J.; Johnson, K.L. A Review of Fluorescence in Situ Hybridization (FISH): Current Status and Future Prospects. *Biotech Histochem* **2000**, *75*, 54–78, doi:10.3109/10520290009064150.